POLITECNICO DI MILANO
Faculty of Industrial and Information Engineering
M.Sc. in Mechanical Engineering

Functional Characterization of Laser Annealed Nitinol Wires

Supervisor: Prof. Carlo Alberto BIFFI
Co-supervisors: Dr. Ausonio TUISSI

M.Sc. thesis of:
Tayebeh Zohari matr. 786202

Academic Year 2014-2015

Table of Contents

Acknowledgements

This thesis is the conclusion of my master graduation in mechanical engineering, at university of Politecnico di Milano. Here I wish to thank all the people who have contributed to my growth, both professional and personal, during these years.
First of all, I would like to thank the beautiful country, Italy, and its nice people for all amazing moments I had during the years of my study.

My sincere gratitude to my thesis supervisor Doctor Carlo Alberto Biffi for his trust and supports in any step of this project. Many thanks to all the stuff of the CNR who helped me through my work kindly and patiently.

I am also thankful to all my friends and classmates who made this period of study full of memorable moments for me.

The last but not the least, the biggest thanks goes to my family, whom without their love and support I was not where I am. Thanks to my parents, Mehdi Zohari and Farideh Khosravi and my dear sister, Sahereh for supporting and encouraging me to follow my goals.

List of Figures

List of Tables

Abstract

Shape memory alloys are functional materials, able to offer a unique mix of different properties: the shape memory effect and the pseudo-elasticity. Due to the reversible solid state martensitic transformation, these two properties can be found in this class of materials. These alloys require a specific annealing, called shape setting, in order to fix their principal properties; this treatment is usually done by using furnaces.
This thesis work is based on the study of a new approach to perform the annealing on a pseudo-elastic NiTinol thin wire by using an Ytterbium active fiber laser source.
The effect of laser power and process speed has been studied on the martensitic transformation and on the mechanical properties of the thin wires.
The characterization of the wires were performed through differential scanning calorimetry, stress-strain tests, done at room temperature, and microstructural analysis. The obtained results were then compared to the performances of the commercially available wires, which were conventionally heat treated in oven. It was found that the wires laser annealed shown at least comparable properties of the commercial wires, obtained by conventional techniques. Due to rapid heating and cooling of laser treatment, the wires' properties can be evidently improved by the generation of a microstructure, orientated along the wire length, more than the one obtained by furnace.
Moreover, the modulation of the functional properties of the NiTinol can be done by changing the incident power.
It can be concluded that the NiTinol pseudo-elastic wires, annealed by unconventional laser technology, can be proposed and potentially used for biomedical applications and the laser technology can be a real competitor of conventional thermal treatments for this materials.

Keywords: NiTinol, shape memory alloys, pseudo-elasticity, laser annealing, fiber laser, mechanical characterization, differential scanning calorimetry, biomedical applications.

Parole chiave: NiTinol, materiali a memoria di forma, pseudo-elasticità, trattamenti termici laser, laser in fibra, caratterizzazione meccanica, calorimetria differenziale a scansione, applicazioni biomedicali.

Chapter 1

1 Shape memory alloys

1.1 Brief historical overview

Shape Memory Alloys (SMAs) are very interesting materials, which have the ability to memorize and recover their predefined shape and the ability of recovering strains up to 8-10%. This kind of materials has two special properties that have raised from the reversible phase transformations between austenite and martensite. The first SMA was discovered by Olander in 1932. He determined that the gold-cadmium (Au-Cd) alloys could be plastically deformed when cool and return to the original shape when heated. The same effect was discovered in Cu-Zn in 1950s. However, the importance of shape memory materials was not recognized until William J. Buehler and Frederick Wang discovered the quasi-equiatomic NiTi alloy properties during research at the Naval Ordinance Laboratory in 1962. This NiTi alloy is also known as NiTinol, which is derived from its composition and its place of discovery [1]. So, the demand for SMAs for industrial and technical applications has been increasing.
Shape memory effect later was found in copper-based and iron-based alloys, such as Fe–Mn–Si, Cu–Zn–Al and Cu–Al–Ni; due to their impracticability and poor thermo-mechanic performances, NiTi-based SMAs are more popular for most of the applications [2].

1.2 Microscopic behavior

1.2.1 Crystal lattice structure

SMAs are characterized by a martensitic phase transformation, whichoccurs between two solid state phases: a parent phase, called austenite, and a higher disordered phase, called martensite (see Fig. 1-1).
The austenite is the stable state at high temperature and has a body-centered cubic crystal structure (usually B2 for NiTi alloys). It has high symmetry, which corresponds a high elastic modulus.
The martensite phase was named after the founding done by Adolf Martens (1850-1914), a German metallurgist who found the martensitic structure in steel for the first time [3]. It is a low temperature phase and in the NiTi system the martensite has a monoclinic distorted structure (denoted by B19'). The crystal

structure of martensite has a lower symmetry than the austenite phase, and it shows a lower elastic modulus. Since lower symmetry, multiple formations of martensites with the same structure in different orientations are possible; these are called variants. The martensites variants are twentyfour and in a state without any load applied all of them are present.

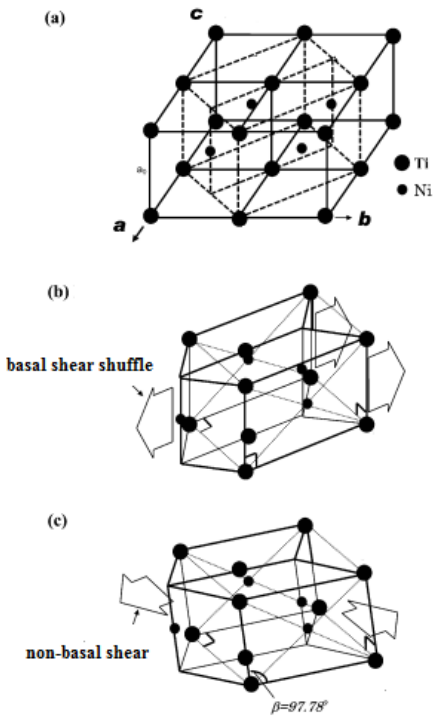

Fig. 1-1: Structure of (a) the parent phase B2,structure with FCT cell delineated , (b) orthorhombic phase B19,formed by shear shuffle of basal plane and (c) the product monoclinic martensite phase B19', which is viewed as a B19 structure sheared by a non-basal plane

Fig. 1-1 shows the structure relationship among B2 (Fig. 1-1.(a)), B19 (Fig. 1-1.(b)) and B19' (Fig. 1-1.(c)). Usually, most martensite structures are derived from different stacking of the basal plane of the parent phase. Considering a face centered tetragonal cell within the B2 structure (Fig. 1-1.(a)) and applying a sliding, it forms an orthorhombic B19 structure (Fig. 1-2.(b)). If additional transverse shear is applied to B19, this orthorhombic structure deforms into monoclinic B19' structure (Fig. 1-1.(c)) [1].

Depending on composition and thermo-mechanical treatment, the martensite transformation can occur in a direct B2→ B19' or in two step B2→B19→ B19' or B2→R→ B19'. This last case is characterized by the onset of the ortorhombic phase (R-phase). There are three cases, in which the R-phase transformation occurs: (1) a few % of Ni in Ti-50Ni alloy is substituted by Fe or Al; (2) Ni-rich Ti-Ni alloys are aged at proper temperatures (say 400 °C) to cause the precipitation of Ti_3Ni_4 phase; (3) heat treatment of Ti-Ni alloys after cold-working to create rearranged dislocation structures.
The lattice of the R-phase was reported to be tetragonal one time, now it is recognized rhombohedral distortion upon the transformation from X-ray powder diffraction patterns.

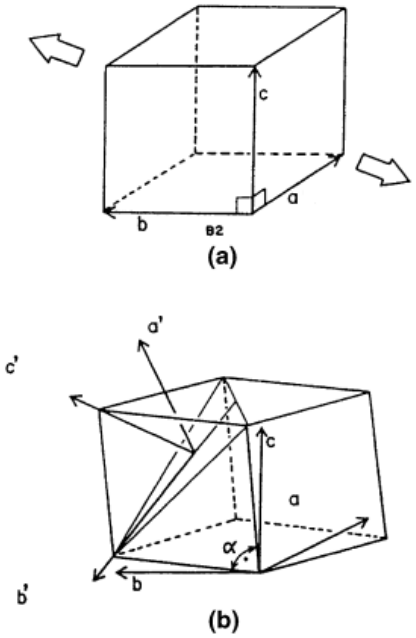

Fig. 1-2: Lattice change from B2 to R-phase. The axes a0, b0 and c0 represent the principal axes in that lattice deformation.

1.2.2 Mechanism of transformation

In general, in the solid state materials there are two types of phase transformations: diffusion and diffusionless (dissipative). In diffusional transformation the new phases, which are formed usually have different chemical composition with respect to that one of the parent phase: this phenomenon happens due to rearranging of atoms in long distances. In the diffusionless transformation the atoms move as a unit, when the overall

displacement is the sum of small movements of each atom. In this mode of transformation the chemical composition of the austenitic parent phase remains intact, since the bond between atoms are rearranged rather than broken. The martensitic transformation is based on diffusionless transformation [4].
This transformation, which is described by a shear-like mechanism, is divided in two parts: the Bain strain and the lattice-invariant shear [5].
The Bain strain consists of the necessary atomic movements needed to obtain the new martensitic structure. This process is represented as a two-dimensional approach, as shown in Fig. 1-3.

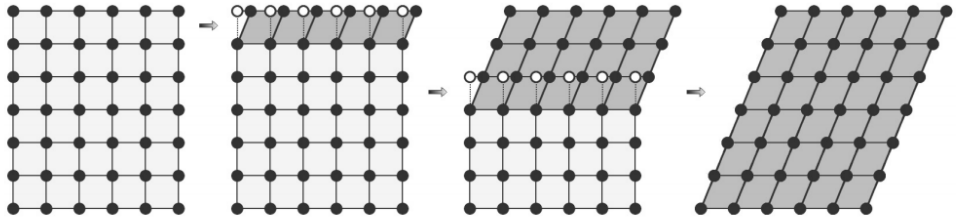

Fig. 1-3: Bain strain movement

Since the Bain strain, that generates the martensite lattice, is not an invariant plane strain, it should be accompanied by other deformation processes that do not distort the martensite lattice but make the resultant of all the strains in invariant plane strain. This is achieved by a lattice invariant shear mechanism, which has two possible routs: slip and twinning [4]. In both the cases, each individual cell has the new martensitic structure but the overall shape is that of the original austenite.
The slipping mechanism can accommodate the change in volume and shape but it is a permanent process, because it breaks some bonds between the unit atomic cells in the new formed martensite, so the change will be irreversible. Instead, twinning is a reversible process; it keeps the parent phase bonds and only makes some variations in shape.

Fig. 1-4: The two mechanism of accommodation: (a) slipping, (b) twinning [6]

Shape memory is a reversible phenomenon, so the twinning is the dominant accommodation process for it.
The SMA, containing 100% of lattice twins, can be easily deformed through variant reorientation (detwinning process). Since the twin boundaries have very low energy, if a stress is applied to the structure, the twin boundaries will easily move, producing a shape modifition, which better accommodates the applied stress. This phenomenon through which many twin variants are harvested to single variant is called detwinning [7].

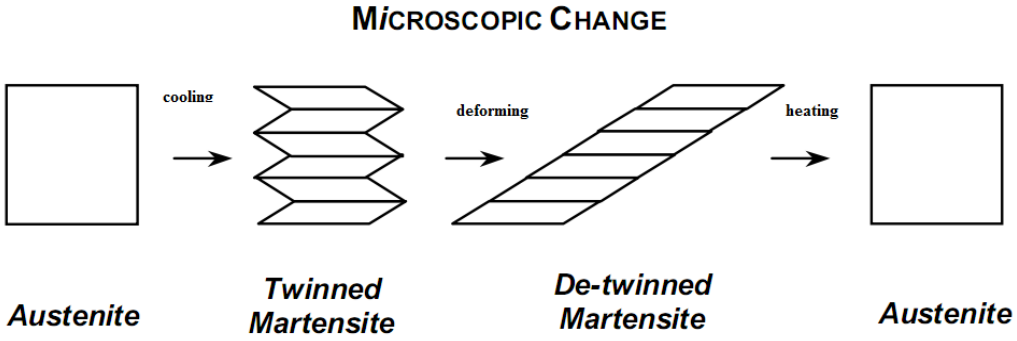

Fig. 1-5: Schematic illustration of martensitic deformation and microstructural changes in SMAs [8]

1.3 Macroscopic behavior of shape memory alloys

The martensitic transformation is divided into two categories: thermos-elastic and non-thermoelastic. The thermoelastic transformation is characterized by a small temperature hysteresis (a few to several tens of degrees), a mobile twin interface, and a crystallographically reversible transformation (and vice-versa for the non-thermoelastic transformation). The shape memory and the pseudo-elastic effects, described in this section, are characteristic of the thermoelastic transformation.
Practically, SMAs can exist in two different phases with three different crystal structures (i.e. twinned martensite, detwinned martensite and austenite) and six possible transformations. The austenite structure is stable at high temperature and the martensite structure is stable at lower temperature. When a SMA is heated, it begins to transform from martensite into the austenite phase.
The austenite start temperature (As) is the temperature at which this transformation starts and the austenite finish temperature (Af) is the temperature at which the transformation in austenite is completed. Once a SMA is heated beyond As, it begins to contract and to transform into the austenite structure (recover its original form).This transformation is possible even under high

applied loads, and therefore, it results in high actuation energy densities. During the cooling process, the transformation starts to revert into martensite at martensite start temperature (Ms) and is completed when it reaches the martensite finish temperature (Mf) [9].
Temperature at which martensite cannot be stress induced is called Md, and above this temperature the SMA is permanently deformed like any ordinary metallic material, losing the pseudo-elastic behavior [10].
Both pseudo-elasticity and shape memory effect occur in the same specimen, and which occurs depends only upon the testing temperature [11]. This situation is illustrated in Fig. 1-6, in which two solid lines and a broken line are drawn.

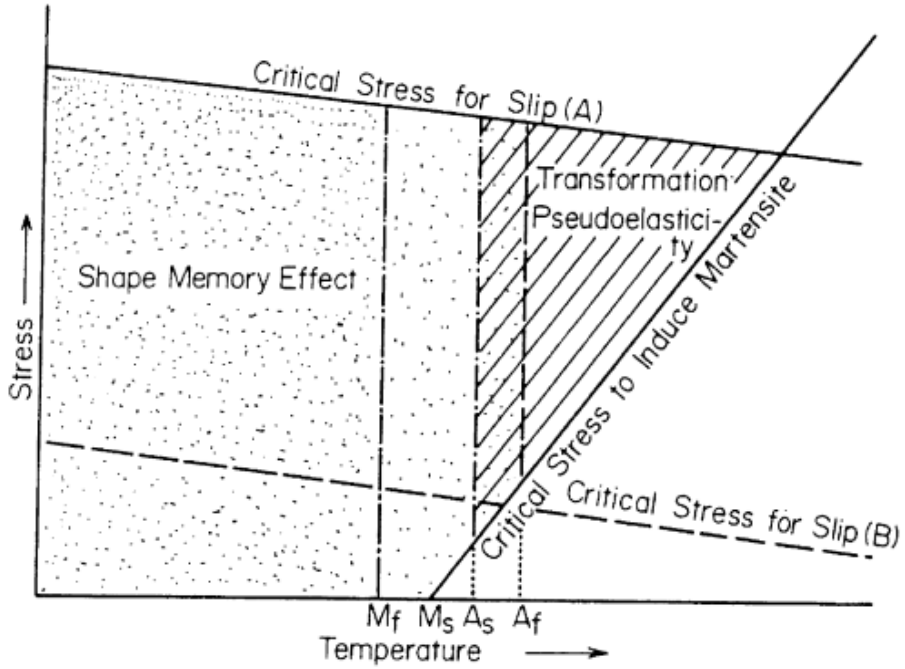

Fig. 1-6: Schematic of the shape memory effect and the pseudo-elasticity [11]

The line with a positive slope represents the critical stress to induce martensite. The lines with a negative slope represents the critical stress for slip. If the critical stress is very low, we cannot expect good or complete pseudo-elasticity, because slip, which is an irreversible process, is easily introduced below the critical stress for stress-induced transformation. Here, we can see that pseudo-elasticity appears at temperatures above Af in the shaded region, because if a stress is applied at temperatures above Af, the stress-induced transformation occurs at a stress above the critical stress for inducing martensite. However, the reverse transformation must occur upon unloading, since the formed martensite

is completely unstable at temperatures above Af in the absence of stress. Thus, we can obtain pseudo-elasticity upon unloading as far as the reverse transformation is crystallographically reversible. Similarly, at temperatures below As, the deformed martensites are stable and thus the martensites stay deformed (or bent) after the release of stress and the strain can recover only by reverse transformation. In the temperature regime between As and Af the martensites are partly unstable and thus both pseudo-elasticity and shape memory effect coexist [12].

1.3.1 Pseudo-elasticity

If the sample is stressed at a temperature above As, then we will get the result similar to that one shown in Fig. 1-7.

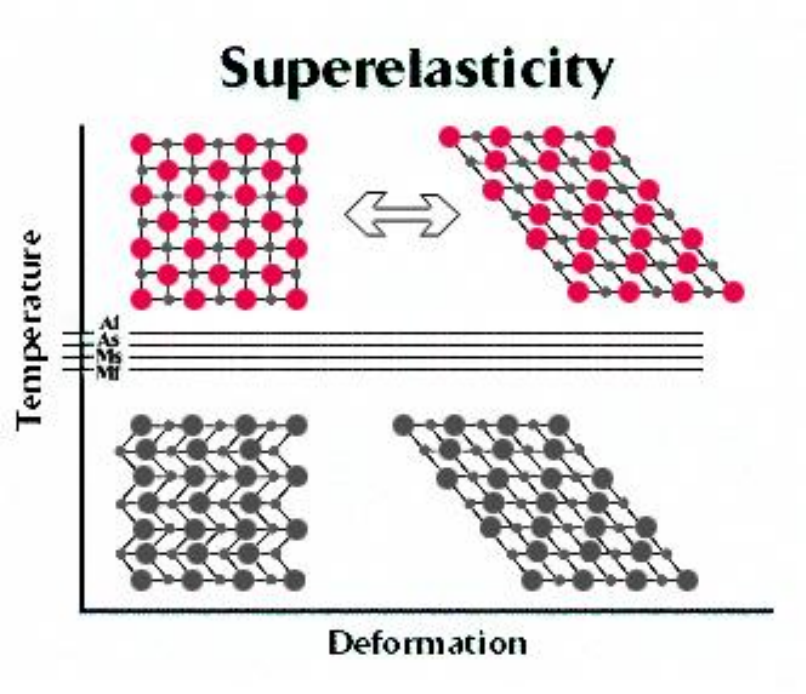

Fig. 1-7: Schematic of the pseudo-elasticity

Since the martensitic transformation occurs by a shear-like mechanism, it is possible to induce it even above Ms, if we apply stress. This is called a stress-induced martensitic transformation and stress induced martensite (SIM) can be consequently generated.
It is also possible to stress-induce the transformation even above Af, if slip does not occur under the applied stress. However, the martensite is completely

unstable at a temperature above Af in the absence of stress. Thus, the reverse transformation must occur during unloading in this case and the strain completely recovers in the thermoelastic transformation, if slip is not involved in the process. Thus, a high critical stress for slip is very important for the realization of the pseudo-elasticity.

The mechanical behavior of the process is displayed in Fig. 1-8. Here again the first range is the elastic one. It should be noted that the martensitic structure can deform by moving twin boundaries, which are quite mobile, thus the yield strength of the martensite is extremely low compared to that of the austenite, which must deform only by elastic deformation of the crystal structure. After the elastic field SIM is formed, leading to the usual pseudoelastic loop with an upper and lower plateau, related to thermal hysteresis and showing an increasing strain at constant stress, related to thermal hysteresis. The upper plateau corresponds to the formation of martensite under stress while the lower one represents the reversion of the SIM when the stress is released [13].

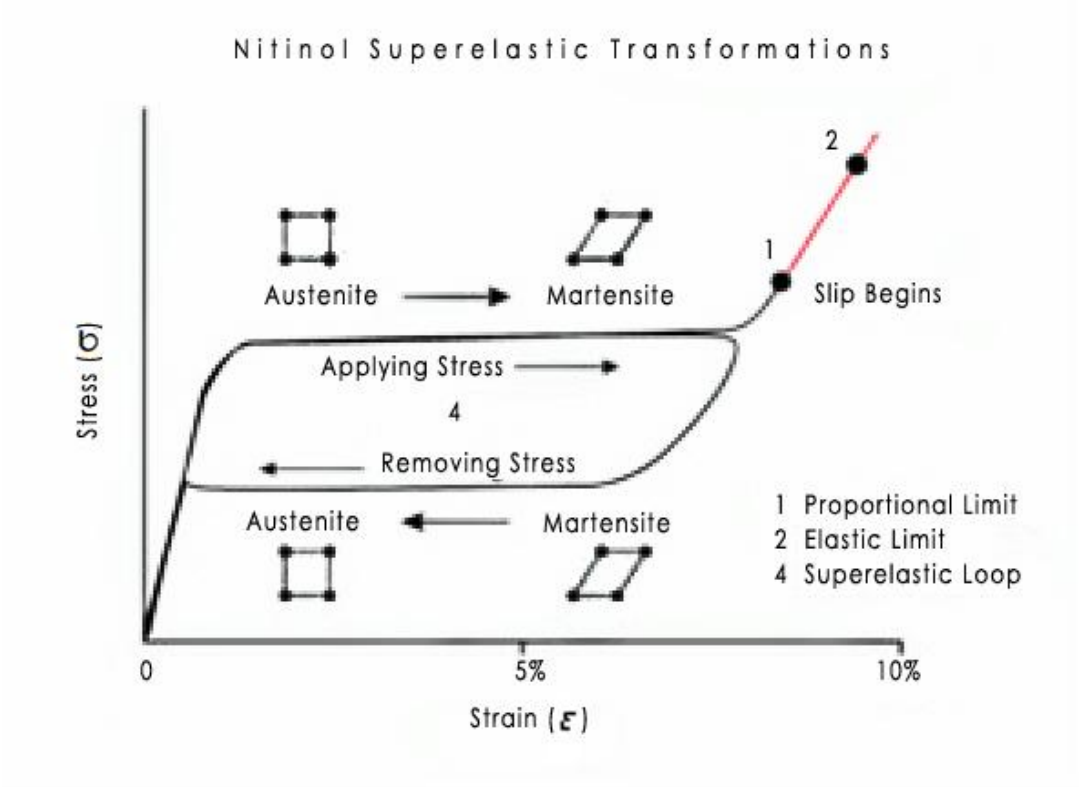

Fig. 1-8: Schematic of the stress-strain curve showing the pseudo-elasticity

1.3.2 Shape memory effect

The phenomenon of the shape memory effect is clearly demonstrated in photographs of Fig. 1-9, where the evolution of the shape of a NiTi wire is depicted. The wire is martensitic at ambient temperature, therefore the wire in the martensitic state (1), whose shape is the same as in the parent phase, is deformed at ambient temperature (2). However, it will revert to its original shape by means of the reverse transformation (3)-(5), if it is heated to a temperature above A_f.

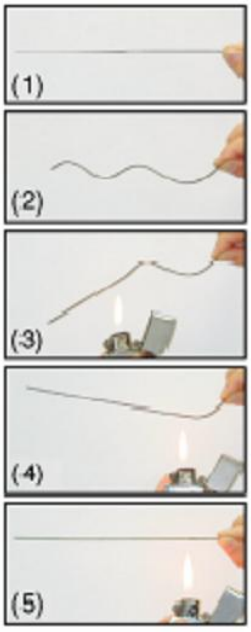

Fig. 1-9: Schematic of the shape memory effect [14]

The mechanism of this phenomenon is explained in Fig. 1-10. When the parent phase is cooled below Mf, martensite variants are formed side by side, as shown in Fig. 1-10, as a result of the self-accommodation. If a stress is applied, the deformation proceeds by twin boundary movement. If, however, the sample is heated to a temperature above Af, the martensite variants are rearr [14]anged under stress revert to their original orientation in the parent phase. This effect is usually called as the one-way shape memory [15].

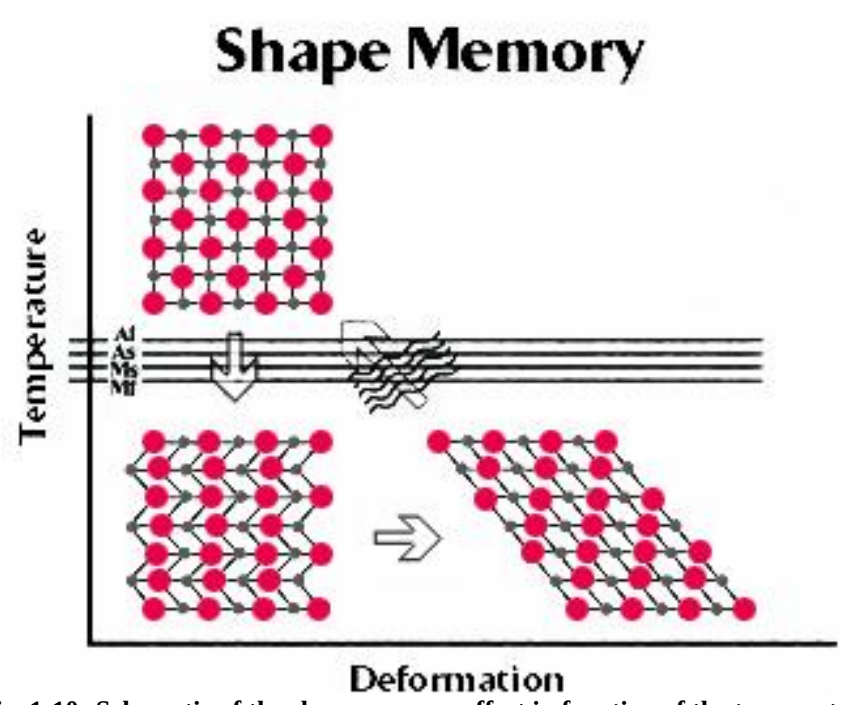

Fig. 1-10: Schematic of the shape memory effect in function of the temperature

In addition to the one-way shape memory effect (OWSME), a two-way shape memory effect (TWSME) indicates that the material can remember its shape at both the high temperature (for the austenite) and the low temperature (for the martensite). However, TWSME is less applied commercially due to the 'training' requirements and to the fact that it usually produces about half of the recovery strain provided by OWSME for the same material; moreover, the strain tends to deteriorate quickly, especially at high temperatures. Therefore, OWSME can provide a more reliable and economical solution.

Otsuka provides an explanation for the TWSMA. As shown in Fig. 1-11, when the applied stress is small, the specimen returns to the original shape completely by SME (a-c). However, when the applied stress is too large (d), irreversible slip occurs and it is impossible for it to come back to its initial condition. However, in the next cooling cycle, the specimen elongates automatically as shown in (f). Then, if heating and cooling is repeated, the specimen changes its shape between (g) and (f), respectively. The specimen now remembers the shape of (f) in the martensitic state: this is evidence of the TWSME [4].

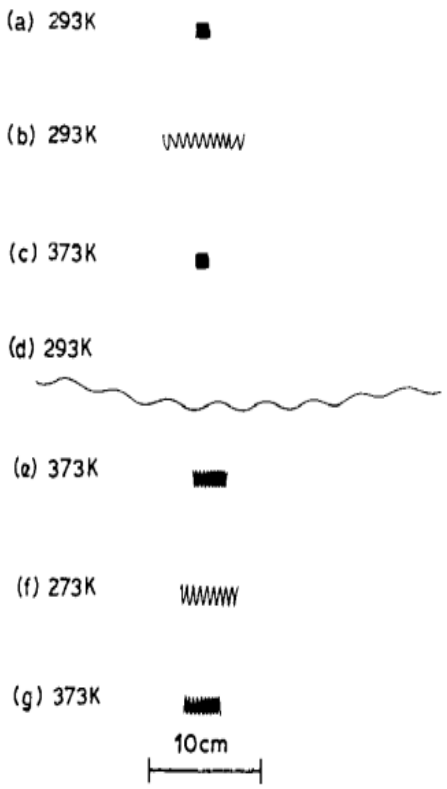

Fig. 1-11: Schematic of the TWSME

1.4 Niti based shape memory alloy

SMAs based on Nickel and Titanium has provided the best combination of material properties for most of the commercial applications. The discovery of shape memory properties in NiTi system was done in the 1960's; it led to the rapid growth of interest in the shape memory phenomenon. Today, a series of extensive reports have been documented the properties of NiTi, mainly in wire form, and provided useful information for designers.

1.4.1 Metallurgy of NiTi

NiTi SMAs are ordered intermetallic compounds, based on the quasi-equiatomic composition. From the phase diagram, shown in Fig. 1-12, this compound exists as the stable phase down to room temperature.

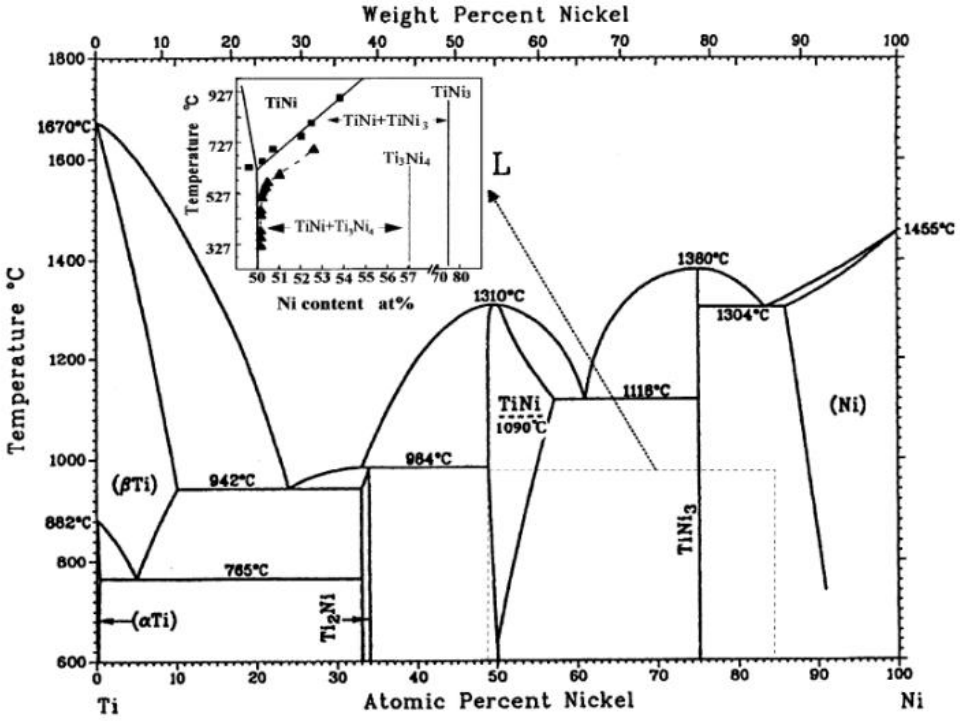

Fig. 1-12: NiTi phase diagram

Consequently, in contrast to Copper based alloys, no betatising and quenching is necessary to prevent the decomposition into other phases at intermediate temperatures. However, at low temperature the stochiometric range of NiTi is very narrow and so the alloys often contain precipitates of secondary intermetallic phases. The microstructure is, therefore, primarily single phase, with small amounts of other phases distributed in the matrix. One factor, which is often ignored in considering the microstructure of NiTi alloys, is the presence of oxygen. Titanium is very reactive, particularly in the molten state, and some parts of oxygen content is present in the alloy. From the Ni-Ti-O phase diagram, oxygen decreases the stoichiometric range of the NiTi compound and can unexpectedly result in compositions within a three phase field. Thus, Ni3Ti can be present, for example, in a titanium rich alloy. Moreover, the oxide Ti4Ni2O is isostructural with the intermetallic Ti2Ni6, which can make unique phase

identification difficult. If the composition of the alloy deviates from stoichiometry, then larger precipitates are presents. The larger second phase particles can have a marked effect on the hot workability of the NiTi alloys, particularly on the titanium rich side where they are brittle and often result in cracking.
Within the composition range, at which the NiTi phase exists at ambient temperature, Ms depends quite strongly on the composition (see Fig. 1-13), particularly on the Ni-rich side, Ti-rich alloys show less sensitivity, primarily as result of the formation of a Ti-rich precipitate, leaving the matrix composition essentially the same.

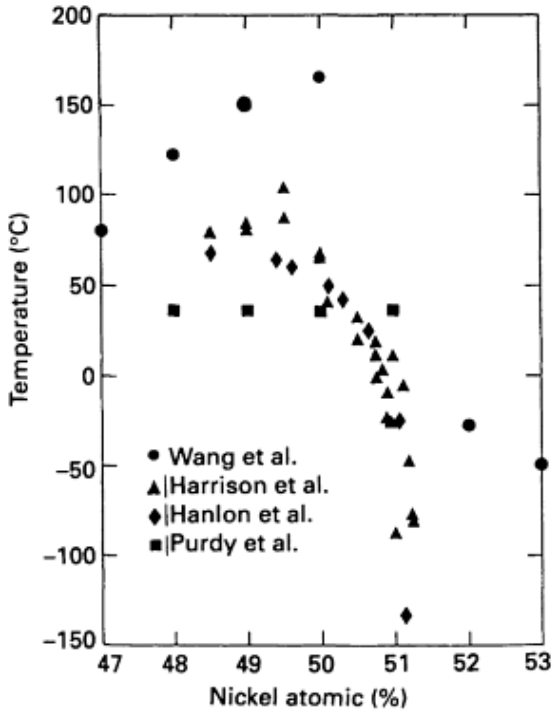

Fig. 1-13: Dependence of the transformation temperature Ms on the composition

The composition dependence of Ms, shown in Fig. 1-13, has an important practical consequence. Precise composition control is required, when melting of the alloys is done for their preparation. Depending upon the desired Ms, the necessary control needs to be done between one tenth and one hundredth of a percent. The compositional accuracy required for SMA NiTi alloys is mostly more precise than the errors in chemical analysis. Therefore, in most of the cases

for quality control purposes the transformation temperature itself is measured rather than the chemical composition.

1.4.2 Mechanical properties

NiTi alloys shows marked differences in mechanical behavior depending on whether they are tested in austenite or the martensite phases. The stress- strain curve of the austenite can be divided into three regions (see Fig. 1-14). An initial low plateau results from the stress induced growth of one martensite orientation at the expense of an adjacent, unfavorably oriented one, this process occurring by detwinning type of mechanism. At higher stresses there is a second region which is usually linear, although not purely elastic. The deformation mechanism in this stage is a mixture of elastic deformation of the detwinned martensite, together with the formation of new orientations of martensite, which intersects those already present, and which provides additional heat recoverable strain. The transition to the third region is a result of the onset of irreversible plastic deformation, as in the case of the yielding of all conventional metals. Therefore, the maximum amount of heat recoverable or memory strain is obtained by initially deforming to the end of stage two. If larger deformation strains are used, then the reversible martensitic deformation processes and the dislocations resulting from plastic flow interact and the memory strain decreases [1].
The length of the martensitic plateau in the stress-strain curve extends typically up to around 5-6%. However, depending on the details of the alloy and particularly its prior thermo-mechanical history, this “plateau” can vary from a continuous curve with an inflection point to a clear horizontal plateau with a sharp yield point and upturn. Because of this variation in yield behavior, many have found it more useful to use a 1% strain offset than a 0.2% offset when defining a yield stress.

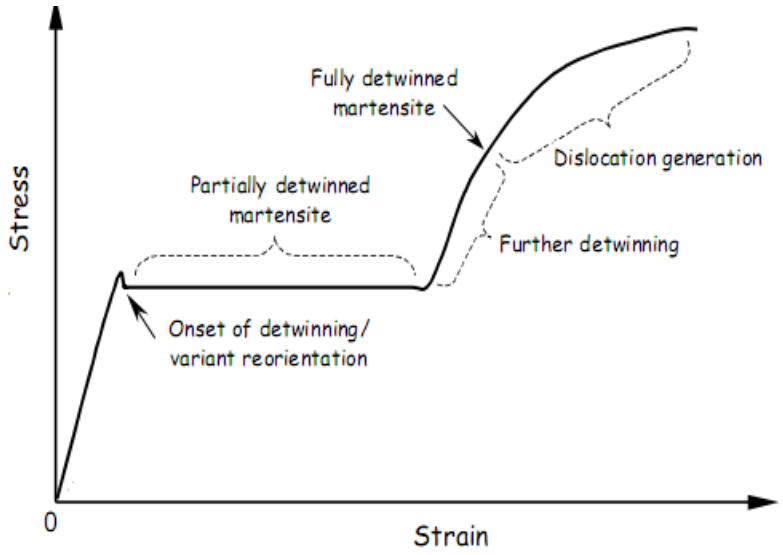

Fig. 1-14: Stress-strain curve of the pseudo-elastic alloy

1.5 Effect of conventional thermo-mechanical treatment

Four years after discovering the shape memory properties in NiTi alloys, a process patent was filled claiming about the cold working in the martensite as a way of increasing the yield strength of the alloy. Since the combination of cold working in martensite together with a subsequent annealing has been extensively explored as a way of improving the SMA characteristics.

Cold working without the annealing step destroys the martensitic plateau on the stress-strain curve. Thus, a material cold worked of 20% in the martensitic state has a very high yield strength but its shape memory properties are poor since only a very low recoverable strain is available. Annealing at spefici temperatures can restore the shape memory effect but decreases the yield stress. Thus, the choice of the amount of cold working and the annealing temperature is a very relevant issue. Cold working introduces a high density of dislocations, which prevent the mobility of twin boundaries. Annealing rearranges these dislocations into cells of relatively dislocation free areas within which the martensite twins can be moved but surrounded by dislocation networks. It is the presence of cells or subboundries, which gives the hardening.

Many researchers have studied the effect of traditional material processing procedures, such as cold working and aging on the thermos-mechanical response of SMAs.

Fig. 1-15 shows the calorimetric curves of NiTi specimens with multiple percentage of cold working, subjected to different annealing temperatures, for

identical time periods: this results in different levels of recrystallization [16]. Moreover, these parameters can even change the characteristic temperatures of the MT. Fig. 1-16 reports the effect of the cold working and the temperature of annealing on the heats exchanged during the MT, which are associated to the amount of the phases involved in the MT. In fact, both the parameters should be carefully selected in order to optimize the functional performances of the alloy.

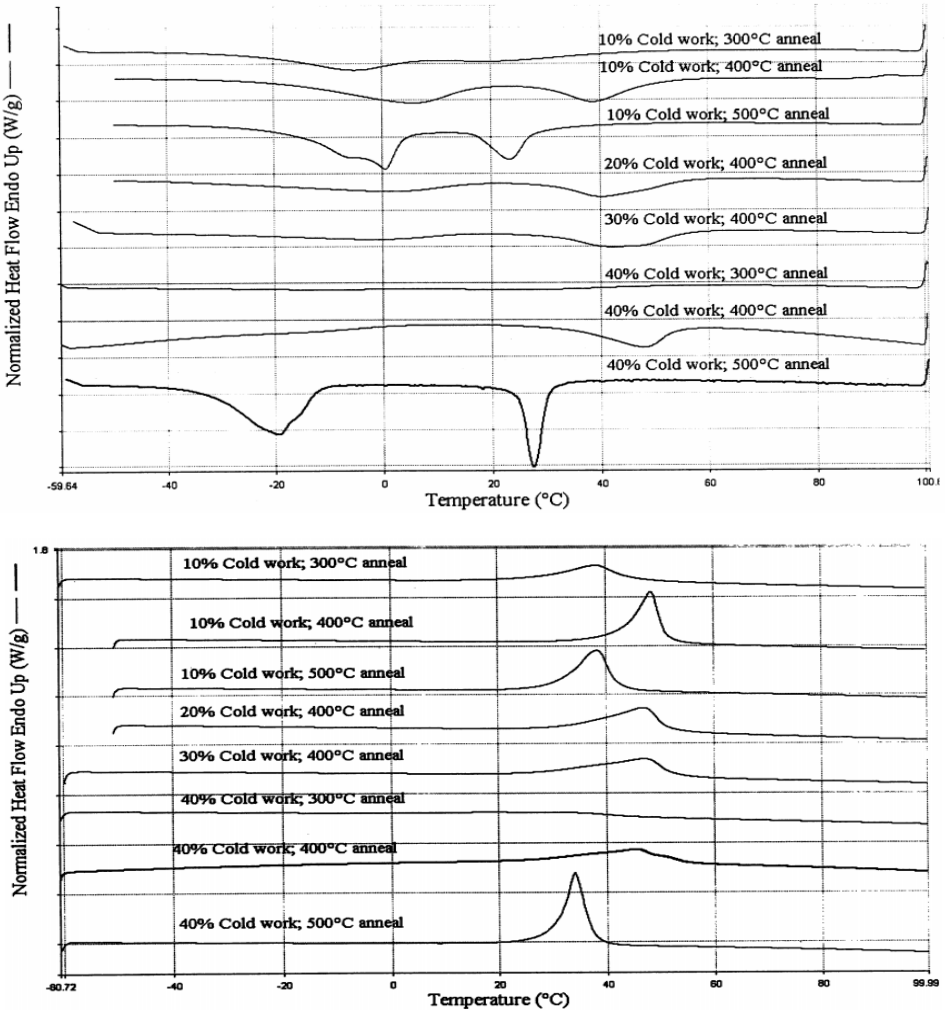

Fig. 1-15: Calorimetric scans of NiTi alloy under different levels of cold working

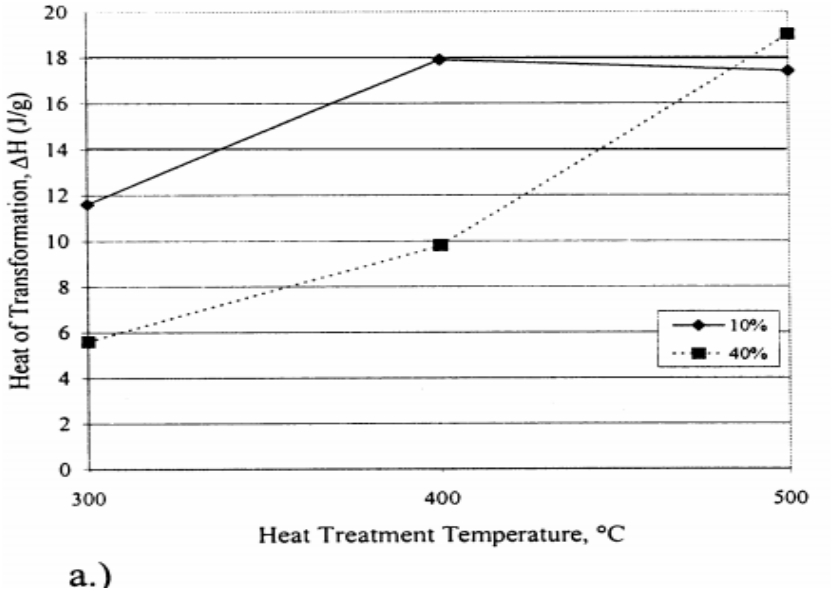

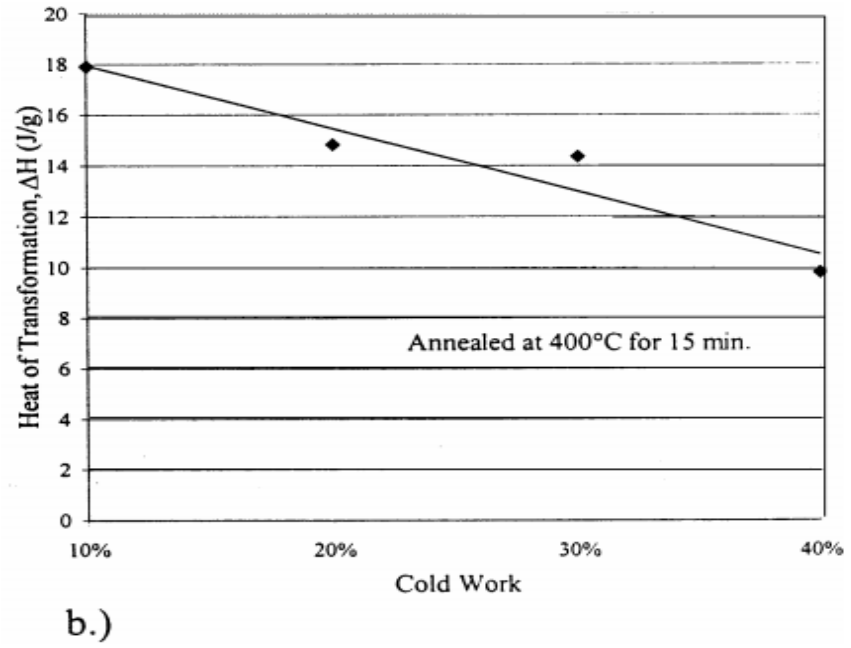

Fig. 1-16:Effect of (a) annealing temperature and (b) cold work on the latent heats of transformation for NiTi specimens [16]

Thermo-mechanical processing, performed in a conventional way by using furnaces, is important for the optimization of pseudo-elastic behavior. Increasing the yield strength of the austenite can widen the temperature range over which martensite can be stress induced without the intervention of plastic deformation. From a mechanical point of view, however, the binary pseudo-elastic alloy is more complicated. If the pseudo-elastic behavior at ambient temperature is required, then Ms has to be lower and the alloy will tend to be nickel rich. Solution treatment followed by rapid cooling and cold working will provide additional hardening from the precipitation of nickel rich phases as a result of the instabilities [17].
Additionally to this, a thermo-mechanical treatment can be even performed after the cold working: in this case it means to apply a stress to the alloy during the annealing. The SMA performances are consequently modified. This aspect becomes important when the application requires the recovery of a specific shape; in this case, the material has to be annealed imposing a certain shape, which can be done by applying an external force. This procedure is usually called shape setting. So, the shape setting process can be considered as the last step of the production route of a SMA material and it is required to fix the functional properties (pseudo-elasticity and/or shape memory effect) and, if necessary, the shape of the semi-finished product (plates, coils, wires) which has to be recovered upon heating above Af for inducing the shape memory effect.

1.6 Unconventional thermo-mechanical treatments

On the contrary with the annealing performed in furnace, there are other methods used to induce the functional properties in the SMAs.
An example of unconventional shape setting is the electrical fast method, where current sparks can quickly heat up the wire by Joule effect and consequently a fast annealing can be induced in the alloy [18]. Good functional properties can be induced, because the rapid thermal treatment can limit the grain size.
Another unconventional method for doing the shape setting can be based on the use of a laser beam. In literature only few works can be found, showing how a laser can be used to make a general annealing or the shape setting on NiTi SMA. Dennis et al. proposed an analytical model for simulating a laser thermal treatment, made on a NiTi wire, 0.6 mm in diameter, [19] while Birnbaum et al. studied the laser forming of thin PE NiTi plates [20] . Anyway, laser technology can be adopted as a preferential and powerful heat source for performing a fast shape setting, able to fix the functional properties of SMAs. Wang et al. studied the annealing by using a laser beam of thin films of amorphous NiTi alloys [21]. On the contrary, Meng et al. have shown how a gradient of different functional properties can be realized by inducing the fusion on the top surface of NiTi plates [22] ; in this way, a gradient of functional properties can be obtained from

the surface, where a thin layer of material is melted, down to the core of the alloy, where the material does experience the heating with decreasing temperatures.

1.7 Applications of shape memory alloys

The remarkable properties of SMAs have promoted several investigations related to their applications in different application fields.
Practical applications for using SMAs appeared within 10 years or so after the discovery of the shape memory effect in Ti-Ni alloys. The first successful application was made by Raychen Corp. for fasteners and tube couplings [23]. Today the most intensive application of SMAs is in the medical area.
In this paragraph we will mostly discussed medical applications and engineering applications of SMAs.

1.7.1 Biomedical application

The use SMAs in medicine is now widely recognized and accepted. Although NiTi alloys are significantly more expensive than stainless steels, SMAs can exhibit excellent behavior for biomedical applications, such as good corrosion resistance, biocompatibility and unique physical properties, like the pseudo-elasticity and the shape memory effect. Fundamentally, NiTinol is an alloy containing approximately the same amount in atomic percentage of Nickel and Titanium. Small compositional changes around this 50:50 atomic ratio make dramatic changes in the operating characteristics of the alloy. Slightly Nickel rich alloys result in the effect of pseudo-elasticity and it is this phenomenon that is utilized in the vast majority of medical applications [14]. The first pseudo-elasticity braces made from a NiTi alloy, introduced by Andreason in 1971 [24].
SMA made a significant breakthrough into biomedical domain after its introduction in minimally invasive surgery (MIS) [25] and more biomedical applications are developed and introduced into the market after the approval of the mitek surgical product (i.e Mitek Anchor) for orthopedic surgery by US Food and Drug Administration (FDA) in 1989.
Nowadays, SMAs are used in medical equipment and devices in many fields, including devices used in orthopedics, neurology, cardiology and interventional radiology.
Probably, the best illustration of all excellent properties of SMAs is also the most celebrated pseudo-elastic medical device: the self-expanding stent [14].
The stent (see Fig. 1-17) is reserved for devices used to scaffold or brace the inside circumference of tubular passages or lumens and most importantly, a host of blood vessels including coronary, carotid, iliac, aorta and femoral arteries.

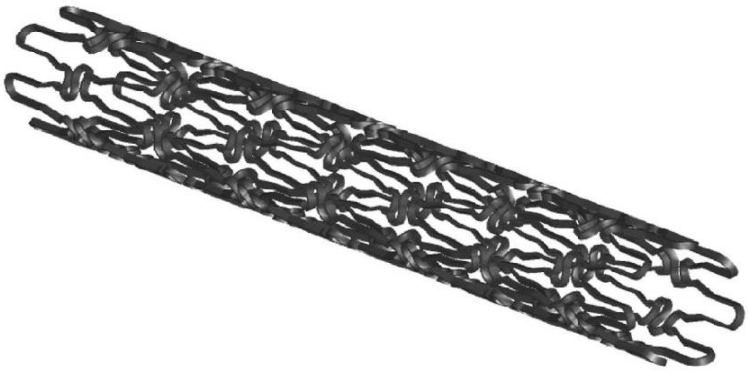

Fig. 1-17 :Model of stent laser cut from NiTinol tube

Stent in the cardiovascular system is often used as a follow-up to balloon as placed in the diseased vessel and expanded in order to reopen a clogged lumen.
Stents can be classified as ballon-expandiable, where the angioplasty balloon is employed to both open the blocked vessel and expand the stent, or as self-expanding. The majority of NiTinol stents are of the self-expanding type, whereas the stent is pushed out of the catheter it immediately opens out to support the already dilated lumen.
Nitinol stents are usually made from laser cutting with following polishing [26].
The pseudo-elasticity of NiTinol was the predominant property in the initial interest for using it in the stent applications.
The hysteresis associated with the pseudo-elastic stress/strain behavior of NiTinol can be exploited in the application and deployment of the stents.
Fig. 1-18 shows how the stress/strain behavior of bone and tendons fits with the hysteresis of NiTinol.
The other aspects of the hysteresis loop that can be exploited in stent applications is that of the upper and lower plateau stress. Fig. 1-19 illustrates how the hysteresis of the pseudo-elastic NiTinol provides an excellent solution to this requirement.
The upper plateau represents the force required to deform and the lower plateau represents the force exerted on the vessel tissue during self-expansion.
With appropriate heat treatments and alloy selection the plateau may be finely tuned for the specific stent application.

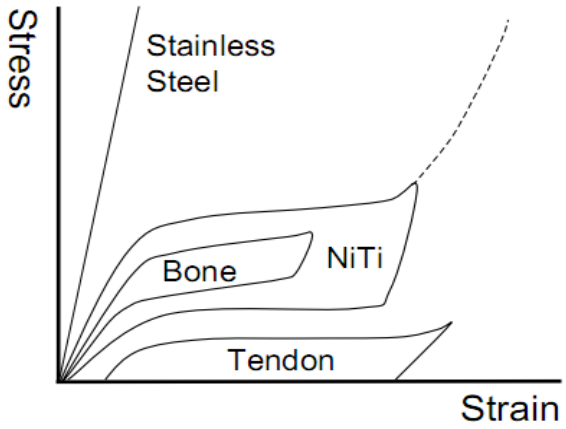

Fig. 1-18-The stress vs. strain relationship for superelastic nitinol, stainless steel, bone and tendon tissue [14]

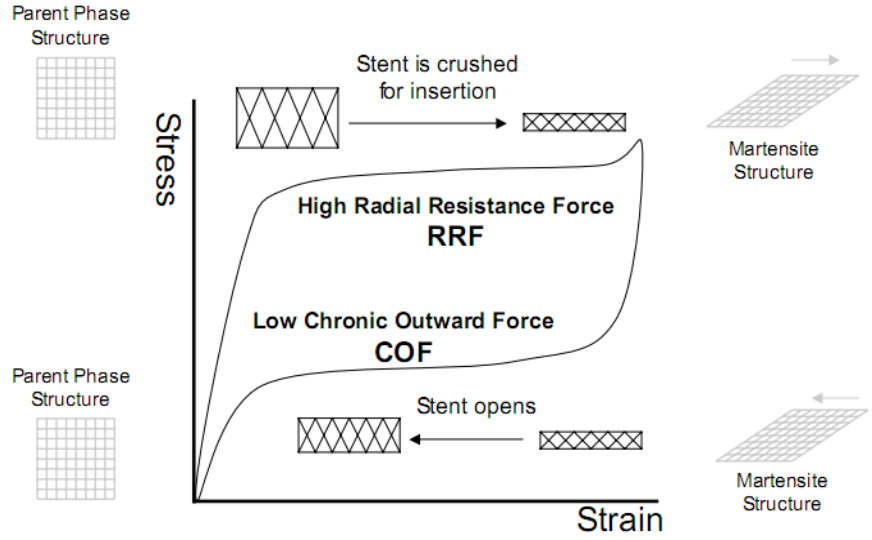

Fig. 1-19:The radial resistive force and chronic outward force as a function of the pseudo-elastic hysteresis loop [14]

Another application of SMAs is in orthopedic for spinal vertebrae spacer (see Fig. 1-20). The use of a shape memory spacer permits the application of a constant load regardless of the position of the patient who preserve some degree of freedom. Fig. 1-20 shows a spinal vertebra and a shape memory spacer on the left side the spacer is in the martensitic state, and on the right side, the spacer is in its original shape, recovered by the pseudo-elastic phenomenon.

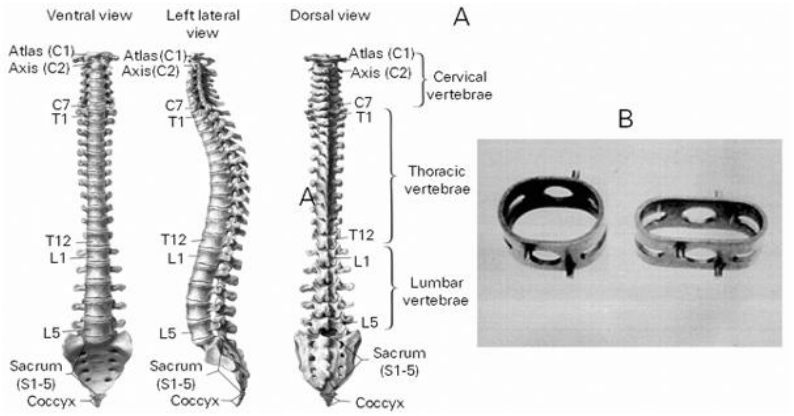

Fig. 1-20:Spinal vertebrae spacer in SMA

Shape memory plates also can be used for the substitution of bones as prosthesis. They are placed in the fractures and fixed with screws. Because of the shape memory effect, when heated these plates tend to recover their former shape, exerting a constant force that tends to join parts separated by fractures (Fig. 1-21).

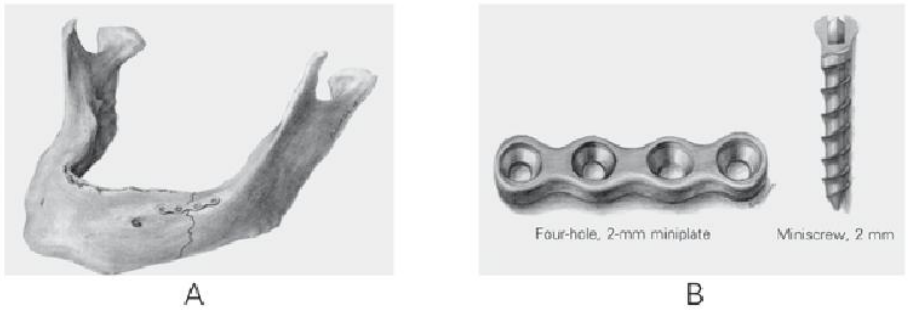

Fig. 1-21: Shape memory bone plates. A, plates fixed upon a human jaw. B, detail of the plate and the screw.

Orthopedic treatments also exploits the properties of SMA in the physiotherapy of semi-standstill muscles [27]. Fig. 1-22 shows gloves, that are composed of shape memory wires on regions of fingers.

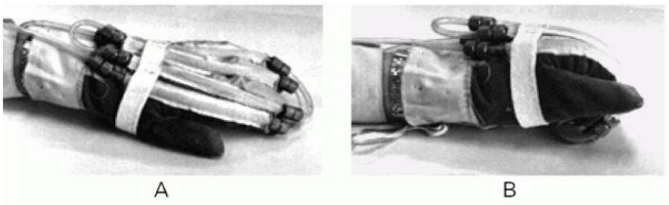

Fig. 1-22: Gloves with SMA wires [27]: (A) position at low temperature; (B) position at high temperature

Orthopedic applications tend to be concerned with shape memory thermal recovery and the associated forces generated during recovery. The research and development has been currently carried out even into porous NiTinol structures, which may perhaps open the door for commercial application of NiTinol in orthopedics [28].
In the recent years medicine and the medical industry have focused on the concept of less invasive surgical procedures.
Following this tendency shape memory instruments are becoming noticeable. Instruments, that are steerable, highless, kink resistant, highly flexible and that provide constant force have also been developed [29] .

1.7.2 Non-medical applications

The diversity of applications using SMAs, apart from the medical field, becomes quite large. The unique behavior of NiTi SMAs have spread new innovative applications in the aerospace, automotive, automation and control, appliance, energy, chemical processing, heating and ventilation, safety and security, and electronics (MEMS devices) industries. Some of these applications apply similar methods, concepts or techniques, which are also applicable for other areas; such as the NiTi thermovariable rate (TVR) springs, which are used to control the opening door in the self-cleaning oven, is also used to offer smooth gear shifting for Mercedes-Benz automatic transmissions, for domestic safety devices to control the hot water flow, and for industrial safety valves to prevent flammable and dangerous gasses from flowing [30]. Some relevant SMA engineering applications and discoveries are summarized in this section.

1.7.2.1 Coupling and fasteners:

Heat-recoverable couplings, heat-to-shrink fasteners, demountable connectors are all applications, making use of the force created by a deformed SMA element during constrained recovery. A full description of the mechanical aspects of constrained recovery is given by Proft and Duerig [31]. In fact, a coupling to connect Titanium hydraulic tubing in the Grumman F-14 air craft, developed by Raychem, was the first large scale application of SMA in 1971 [4]. The original alloy was a Ni–Ti–Fe. Fe was alloyed to obtain a transformation temperature below 55°C. This should prevent that the coupling would transform into martensite at lower temperatures and thus would soften and starts leaking. The concept is straightforward: a sleeve is machined with an I.D, that is approximately 3% smaller than the diameter of the tubing, designed to be joined. It is then cooled to its martensitic state and radially expanded up to 8%, making it large enough to slip over two tube ends. When heated, the sleeve shrinks onto the tube ends and while the generation of a high force joins the tubes. Most couplings are made from cryogenic Ni-Ti-Fe alloys and have to be stored in liquid nitrogen after expansion.
Wide-hysteresis Ni-Ti-Nb alloys have been developed, which can be stored and shipped at room temperature after expansion at low temperatures and have to be heated to 150°C for the installation. These alloys remain in their high strength, austenitic state even after cooling to below -20°C. Fig. 1-23 shows the schematic of the mechanism.

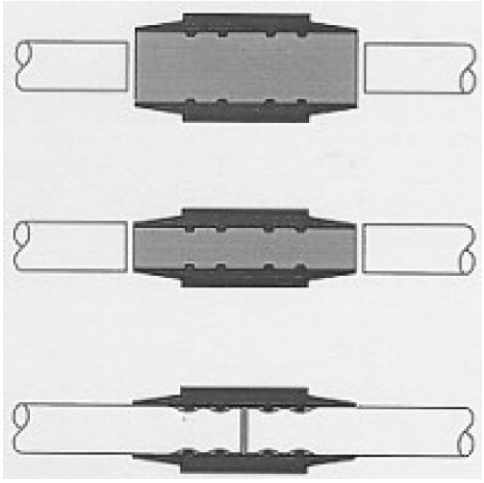

Fig. 1-23: Coupling, machined and expanded(top), after free recovery(middle) and installed on a tube (bottom)

The main advantages of this type of coupling in this particular application is that an easy installation can be performed in difficult areas of access and that the tubing can be placed close together or close to a bulkhead.
The problem of liquid nitrogen storage has been later solved by the stabilization of the martensite, or thermally (in Cu-based alloys) either mechanically (in Ni–Ti–Nb alloys). The development of Ni–Ti–Nb alloys was a real breakthrough for the coupling business but also Fe–Mn–Si alloys received quite a lot of attention in spite of their lower recoverable strain.
The main advantages of these systems are the lightweight, an easy installation even in difficult areas of access, proven reliability, good shock response, vibration and thermal cycling properties can provide a hermetic seal. In the other hand the disadvantages are the high cost relative to classic alternatives, the remaining operational in a limited temperature range (from 20°C up to 200°C) and the limited shape memory amount of motion available.
A special class of couplings or fasteners based on SMA is heat sensitive elements that should lock or unlock two different parts within a short time and at a critical temperature. Those types of applications can be found especially in the area of fire (or excessive heat) protection and release mechanisms in space technology. A typical example is the former Proteus-Link, which replaces fusible heat sensitive links. Reliability and resetting potentials are the main advantages.
In fact, the SMA element is retained here in a non-constrained but deformed martensitic condition.
During heating the one-way effect allows to release the part formerly hold by the SMA device: it can be classified also as a one-way SMA actuator.
Finally, an application that combines unconstrained storage with a constrained action is the static rock breaker [32]. The breaker uses compressively prestrained Ni–Ti rods and can reach recovery stresses up to 950 MPa during heating. The breaker is inserted into a borehole. Significant advantages compared to blasting or mechanical breakers are the safe procedures, the absence of noise, vibrations and dust. It can be used in air, water or other liquids.

1.7.2.2 Smart material

Smart material are defined as those materials that can change their shape and structural characteristics, according to stresses and environmental conditions in which they are located. SMA by themselves are not smart materials. Depending on the goal of their use, they can be classified as adaptive or functional.
Smart materials involve, per definition, three functions: sensor, actuator, control. Those three functions are generally combined by using different materials in combination with a control unit. Combination of several materials leads to

structural elements, that can be called hybrid composites [33]. Hybrid composites connected with a control unit can then be used eventually as a smart structure. The sensing functions of SMA are limited. Temperature changes, if in the appropriate range, will be directly converted in a shape change or a recovery stress. Both effects allow the component, of which the SMA element can be part, to adapt its shape or its performance to the environmental temperature. In case the SMA element is purposely heated, it does not act as a sensor but as an actuator. We should also distinguish between adaptive or smart control by SMA and the performance of SMA embedded in a matrix (hybrid composite). Adaptive control is generally a topic in smart materials sessions but regarding SMA it is an effective use of an SMA element as an actuator. The use of a torsion tube for trailing the edge trim tab control on helicopter rotors is a typical example of the smart blade technology. The main goal of this technology is to reduce noise and vibrations, leading to a higher efficiency and significant noise reduction in the environment.

Another envisaged application is the smart wing for aeroplanes. For similar reasons as in the helicopter rotor blades, the shape of the wing should be adaptive, depending for example on the actual speed of the plane at the same time improving efficiency and noise reduction (see Fig. 1-24). An example of such a wing has been described in SMA adjustable camber (SMAAC). The SMAAC control surface concept is an adjustable camber foil, which is actuated by SMA wires to control the flight of hydrodynamic or aerodynamic vehicles. The SMAAC concept employs a flexible spring backbone, which is actuated by contracting SMA wires and is covered by a pliable elastomer skin to produce an adjustable foil shape.

The advantage of such a system is a much higher lift force than rigid foils in particular cases and a much smaller wake behind the SMAAC foil than the rigid foil at an equivalent lift [34].

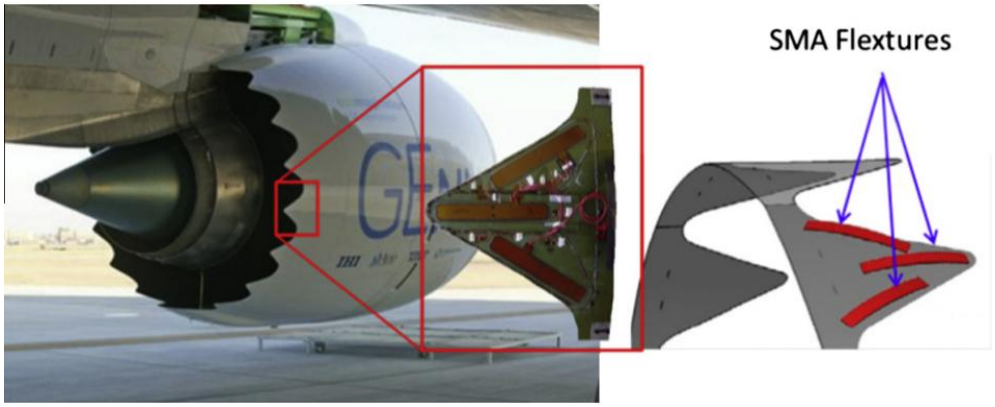

Fig. 1-24: SMA device for noise reduction in jet engines, developed by Boeing and NASA General [35]

1.7.2.3 Robotic application

Since the 1980s, SMAs have been used in a diverse range of commercial robotic systems, especially as micro-actuators or artificial muscles. Today, most of the SMA robotic applications are biologically inspired and widely utilized in biomedical areas but are also used extensively in other fields as well. The primary challenges relevant to the robotics domain are to increase the performance, to reach the miniaturization of the hardware platform and to increase the intelligence of the integrated system (i.e. small, faster, reliable and autonomous). Several technical issues have been highlighted and need to be resolved, such as clamping difficulties, low electrical resistance, miniature electrical connection (for micro-robots), small strain output, control issues and very low efficiency. However, some of these issues have been tackled by selecting suitable modelling techniques, control techniques and feedback sensors. As an example, the resistance feedback control is ideal for micro-robots as it eliminates the necessity of additional sensors, although with limited accuracy [36]. The SMA actuators response rate depends significantly upon its shape and size, and these have a high impact on the overall size and degree of freedom of the robotic device. Resistive heating is generally used for small SMA actuators (up to 0.4 mm in diameter) and indirect heating techniques are applied for thicker actuators. To increase the actuation frequency, capacitors are incorporated with thicker actuators to obtain a rapid heating response and several cooling strategies can be adopted to enhance the cooling process. On the contrary, these would make the device bulkier. Furthermore, to increase the degrees of freedom of the robots, the number of actuators has to be increased, leading to complex control problems.

In a recent review by Kheirikhah et al [37], they divided the robots into several categories based on their locomotion styles and applications such as crawler, jumper, flower, fish, walker, medical and biomimetic robotic hand (see Fig. 1-25). Many robotics researchers are more interested in developing biomimetics and humanoid robots. These robots are useful in solving problems that are challenging for humans, by providing pertinent information from underwater, space, air and land.

Tao et al. [38] designed a robotic fish with a caudal peduncle actuator based on the concept of a FSMA hybrid mechanism that can provide fast response and a strong thrust.

A novel sensory system for robotics has been developed by researchers at Northwestern University, Illinois applying the SE characteristic of a NiTi SMA to create an artificial rat whisker, utilizing the rat's sensing capabilities. The artificial whisker technology has the great potential to enhance robotic sensing capabilities and could be used to examine and navigate into small and tight interior or to locate and identify micro-features on surfaces. Several flying robots have been developed with SMAs, such as the BATMAV and Bat Robot [39]. Recently, a 44 cm length dragonfly with a wingspan of 63 cm was developed by Festo Group, equipped with four SMA actuators to control the movements of its head from side to side and its tail up and down for flight manoeuvre and stability. The 'dragonfly', also known as BionicOpter', has 13 degrees of freedom, can hover in mid-air and movements in all directions.

Fig. 1-25 : Existing and potential SMA applications in robotics domain **[37]**

Chapter 2

2 Aims of the work

In the present work the goal is to study the using of laser technology as an alternative method to the conventional ones to fix the functional properties through shape setting on thin wire of NiTinol SMA. The tests were performed on commercially available pseudo-elastic NiTinol wires, 100 μm in diameter.
Firstly it was decided to identify the feasibility area of the main process parameters, such as the power and the process speed, required for inducing the functional properties.
Secondly, the effect of the process parameters investigated was studied on the calorimetric properties as well as on the mechanical properties of the wires. In details, the characteristic temperature of the martensitic transformation were correlated to the process conditions by means of differential scanning calorimetry; similarly, stress-strain curves, done at room temperature, were associated to the process conditions, showing where the pseudo-elasticity would be induced properly.
The functional performances of the wires, laser annealed, were compared to the ones of the wires, commercially available after conventional annealing.

Chapter 3

3 Experimental

3.1 Material

Smartflex is the trade name of the NiTinol SMA wires, produced by Saes Getters. The material used in this thesis is a wire in NiTinol, 100 μm in diameter; this alloy shows the pseudo-elastic behavior at room temperature, once it is correctly annealed. Table 3-1 reports the main properties of the commercially available wire while Fig. 3-1 and Fig. 3-2 show the calorimetric and mechanical response, reported in the datasheet of the wire, respectively.

Chemistry, %/wt.			
Ni	55.8±0.5	O	0.05 max.
Ti	Remainder	Fe	0.05 max.
C	0.05 max.		
Density		**Melting Point**	
0.235 lb/in³ (6.5 g/cm³)		1300 °C (2372 °F)	

Table 3-1: Main characteristics of the NiTinol wire

Two material conditions were taken into account in this work: (i) cold worked, corresponding to the initial status on which the laser annealing can be performed and (ii) straight annealed, corresponding to the conventional annealing realized by the producer and able to show the functional properties, depicted in Fig. 3-1-Fig. 3-2.

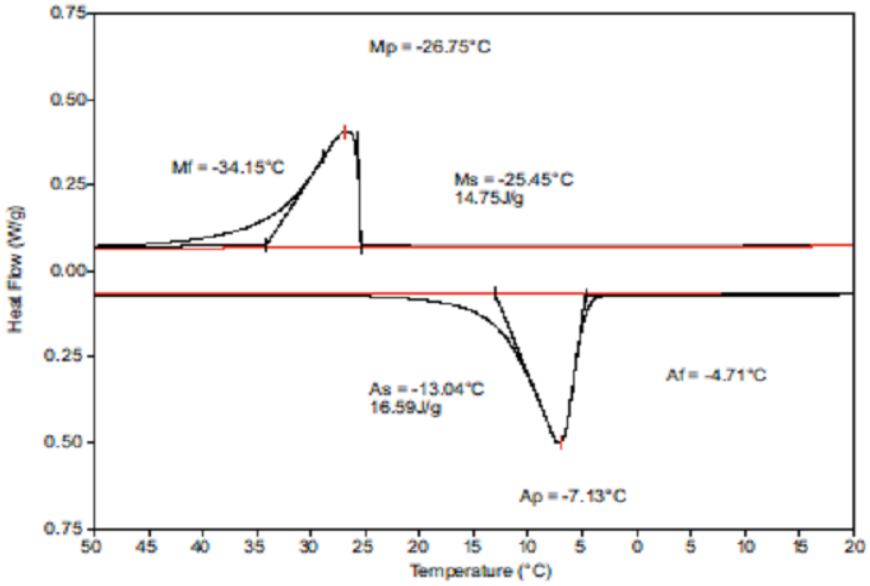

Fig. 3-1:the response calorimetric condition of NiTi smartflex wire

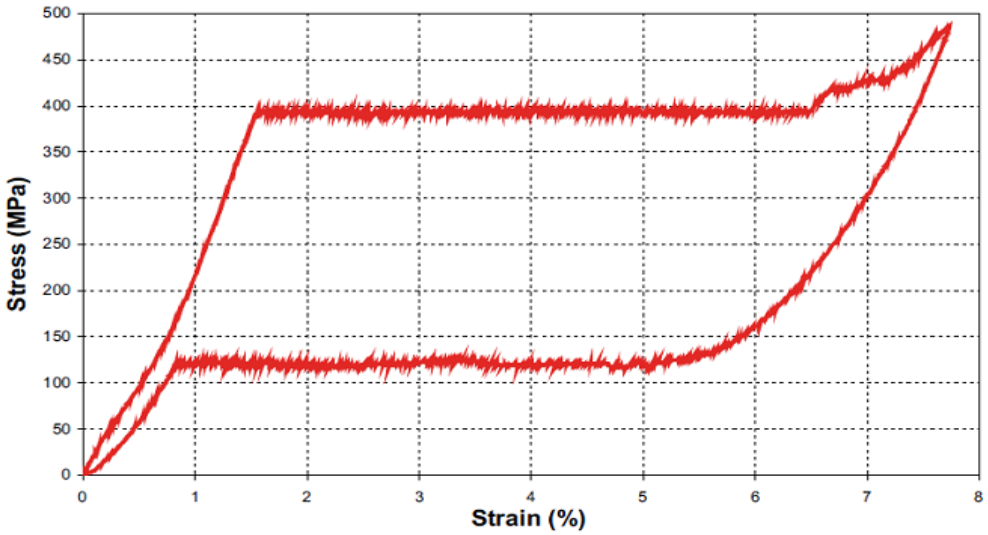

Fig. 3-2: stress strain curve of NiTi smartflex wire

3.2 Laser system:

The laser system employed for this activity is given by an Ytterbium active fiber laser source (model YLR-300/3000-QCW-MM-AC-Y12 from IPG Photonics). The laser source is shown in Fig. 3.3; it can operate in two modes: Continues Wave (CW), having a maximum power of 300 W, and in Quasi Continues Wave (QCW), having a maximum power of 3000 W.
The laser beam in output from the source is collimated and then focalized by using a cutting laser head (model Fiber Mini TM from Laser Mech), characterized by a magnification ratio equal to 2.

Fig. 3-3: Active fiber laser source

The main characteristics of the laser system are summarized in Table 3-2.
The relative displacement between the sample (mobile) and the laser beam (fixed) is controlled through a motion stage (mod. PRO165LM from Aerotech) in two axis x-y, in Fig. 3-4.
In order to complete the degrees of freedom necessary for the management of space three dimensional position of laser beam, two manual slides were provided to manage the displacement along the vertical axis (z axis). The first is characterized with resolution of millimeter for large displacement and the other one with micrometer resolution for precise movement control during the positing of the laser beam.
Finally, a sample holder was design and realized for positioning the wire under the laser beam for performing the laser annealing.
The picture of the entire laser system is shown in Fig. 3-5.

Parameter	Description	Numerical value

λ [nm]	Wavelength	1070
d_{fo} [µm]	Internal fiber diameter	50
BPP	Beam product parameter	1,70
M^2	Beam quality factor	4,99
f_{col} [mm]	Distance of collimation	75
f_{foc} [mm]	Distance of focalization	150
d_o [mm]	Focus diameter	0,10
θ [rad]	Angle of divergence	1,36E-02
Δz_{pdc} [mm]	Depth of field	7,34
P [W]	Maximum power (in CW)	300

Table 3-2: - Main characteristics of the laser system

Fig. 3-4: Motion stage Aerotech - PRO165LM

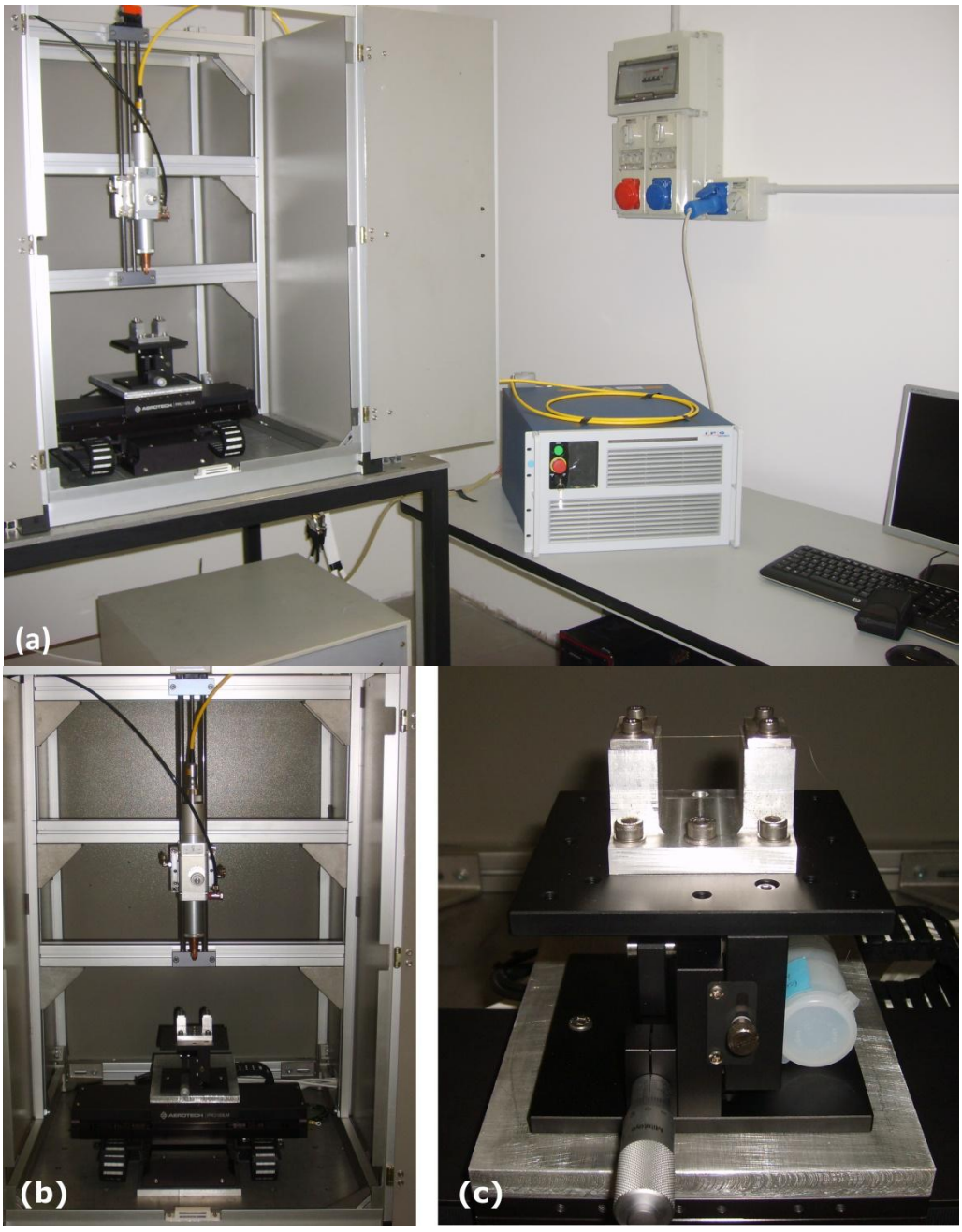

Fig. 3-5: entire laser system used during the experiment

3.3 Laser annealing process

The process of annealing, called even shape setting, have been done on the wire by using the laser beam, according to the schematic shown in Fig. 3-6.

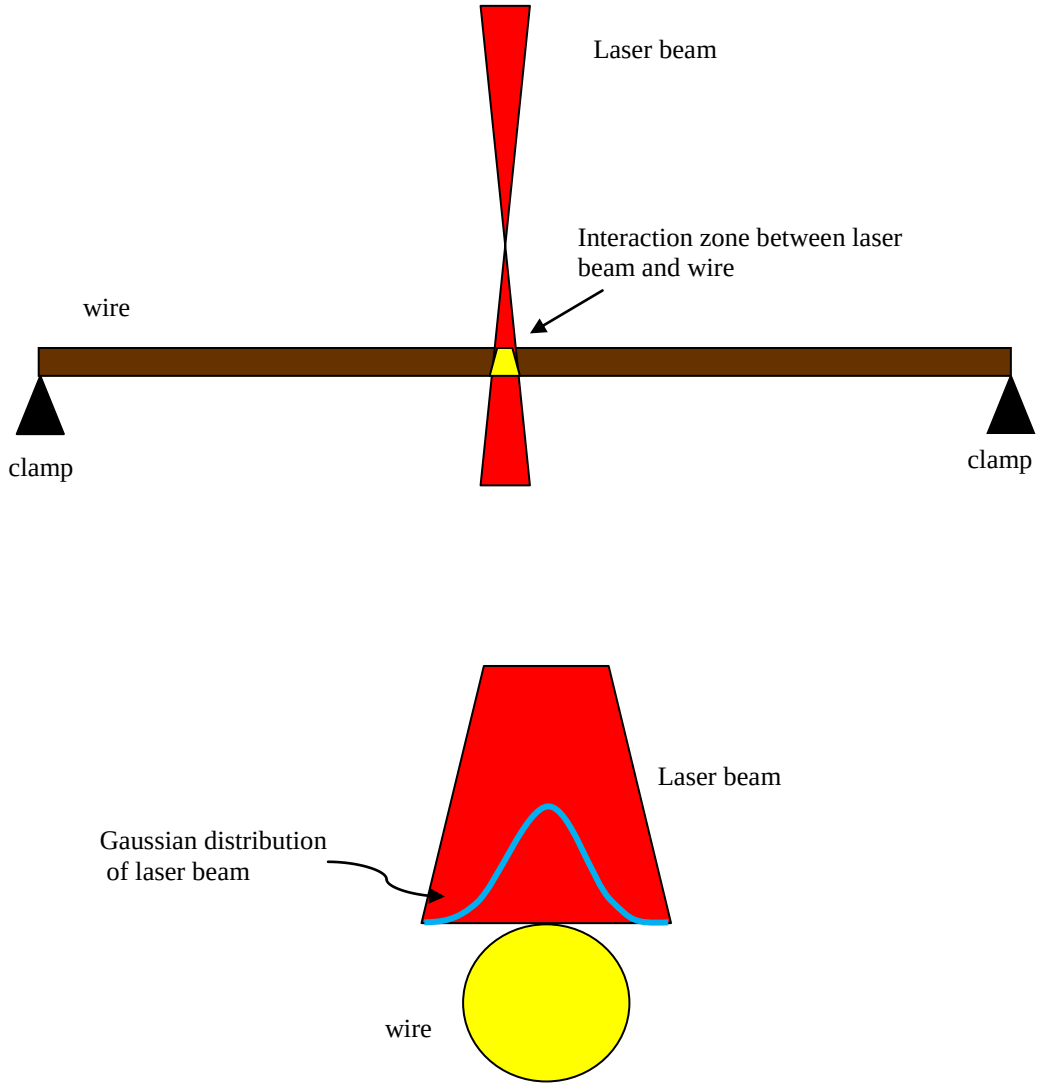

Fig. 3-6: Schematic of the laser annealing process

The laser beam was defocused on the top surface of the wire in order to guarantee an almost flat power distribution. Laser beam, larger than the wire, allowed the positing of the wire under the beam. The wire, 25 mm in length, was maintained straight during the treatment, as shown in Fig. 3-7, and it was moved along a linear path to perform the annealing.

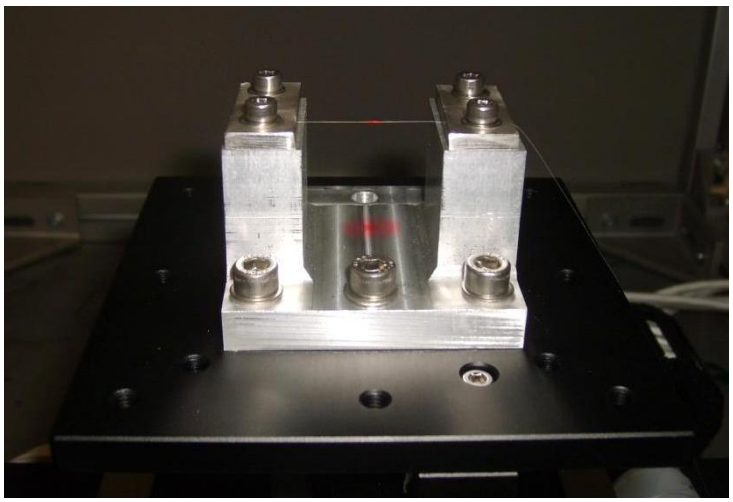

Fig. 3-7:sample holder

3.4 Design of experiments

The experiments were designed in order to identify a feasibility area useful to perform the laser shape setting process. In details, the experimental activity of this work was divided in two steps: the first part was based on the definition of the combination among process speed and power to induced the MT on the samples while the goal of the second one was to study the correlation among the functional properties and the process parameters investigated, such as the laser power and the process speed.
In this paragraph the definition of the path of experiments was defined. The goal of this first set of tests is to identify the process conditions, given by the combination among power and process speed, required to induce the MT as well as the pseudo-elasticity on the wires, in the cold worker condition.
A complete factorial design was defined for studying the effect of both power and process speed. One replication was considered for all the process conditions. The levels of the variable and fixed parameters are listed in Table 3-3 and Table 3-4 respectively. The laser process was not performed in inert atmosphere but just in air.

In details, the range of the power was defined from preliminary test: below the minimum value the MT was not obtained while above the maximum value the melting of the wire was reached.

Variable parameter	Values
Process speed [mm/s]	50-65-80
Power [%]	35-37.5-40-42.5-45-47.5-50-52.5-55-57.5-60
Power range [W]	45-145

Table 3-3: Definition of the variable parameters

Fixed parameter	Value
Laser beam size [mm]	1.3
Focal height [mm]	247

Table 3-4: Definition of the fixed parameters

3.5 Characterization of the results

3.5.1 Differential Scanning Calorimetry

Differential Scanning Calorimetry (DSC) is a thermal analysis technique that monitors heat flow associated with phase transitions and chemical reactions in function of the temperature. These measurement provide qualitative and quantitative information about physical and chemical changes that involve endothermic or exothermic processes, or changes in heat capacity.
The thermal core of a DSC system consists of two cells, a reference and a sample cell, as shown in Fig. 3-8.

Both cells are constructed of platinum to allow high temperature operations. Under each holder a resistance heater and a temperature sensor are present. Current is applied to the two heaters to increase the temperature at the selected rate. A flow of nitrogen gas is maintained over the samples to create a reproducible and dry atmosphere. The nitrogen atmosphere also avoids oxidation of the samples at high temperatures. The sample is sealed into a small aluminum pan and the reference is usually an empty aluminum pan and cover.

During the heating of a sample each peak corresponds to a heat effect associated with a specific process, such as phase change. The first and most direct information obtainable from a DSC curve is the temperature, at which a certain process occurs. The temperature at which a reaction may start is another important parameter. The peak temperature is associated with the temperature at which maximum reaction rate occurs.

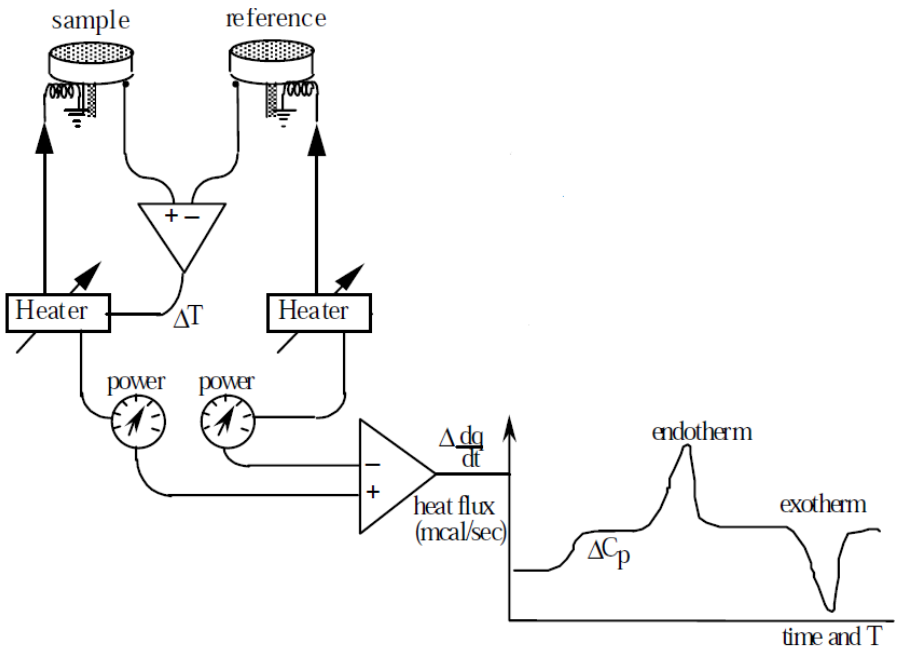

Fig. 3-8: Schematic of the DSC system

During this work a DSC (mod. Q100 from TA Instrument) was used (see Fig. 3-9).
Before starting the experiments, all the samples should be cut into small pieces to fit in aluminum pans. The sample size should be approximately 2-5 mg. The temperature rate was 10 °C/min upon heating and cooling and the range of temperature investigated was between -150 °C up to 150 °C. Each test was done in two loops to approve the stability of the response.

Fig. 3-9: equipment used in this work

A NiTi typical DSC curve is represented in Fig. 3-10. As it can be seen, a complete thermal cycle can cause two exothermic and endothermic peaks respectively. During the transformation from austenite to martensite a product of the first exothermic peak at higher temperature corresponded to the reaction from austenite (A) to R-phase (R), whereas the second exothermic peak at lower temperature corresponded to the reaction from R-phase (R) to martensite (M). Thus, the as-received material on cooling exhibited a well defined two-stage transformation sequence of A→R→M, whereas the A→R peak is narrow and the R→M one is flat and wide. The area under the curve of the peak indicates the heats exchanged or the enthalpy of transformation; moreover, from the DSC scan the start and finish temperatures upon heating and cooling can be measured.

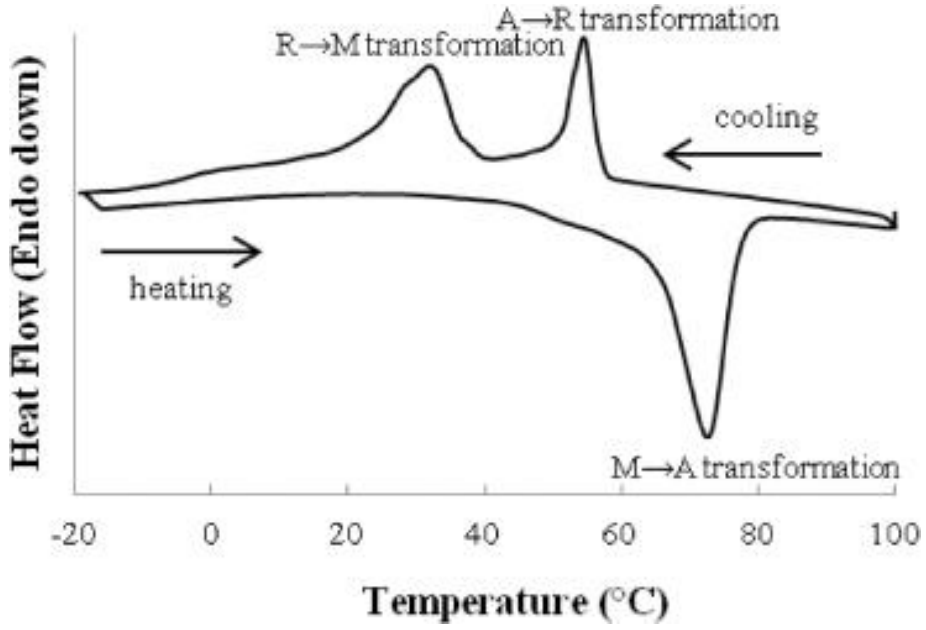

Fig. 3-10: Typical DSC scan of NiTi SMA

3.5.2 Mechanical testing

The mechanical properties of the wires were evaluated from the stress-strain curve by using a Dynamic Mechanical Analyzer (DMA). A tensile test was performed on the straight thin wires at room temperature (25°C) to study the pseudo-elasticity response. Due to the small size of the wires, a fine cell load was required; for doing this job, a DMA with 18 N cell load was adopted. The system used (mod. Q800 from TA Instruments) is shown in Fig. 3-11; the main characteristics of this equipment are listed in Table 3-5.
In order to do the tensile test, the wire is placed inside a chamber. One of the two extremities of the wire is fixed while the other one is placed movable. The specimen is loaded in the DMA with a tensile pre-load. The test were done at room temperature and with the strain rate equal to 1 percent per minute up to 8% of strain and then unloaded.

Fig. 3-11: DMA system used in the experiments

Maximum force	**18 N**
Minimum force	**0.0001N**
Force resolution	**0.00001 N**
Strain resolution	**1 nm**
Modulus range	**103 a 3x1012 Pa**
Modulus precision	**± 1%**
Frequency range	**0.01 to 200 Hz**
Dynamic sample deformation range	**± 0.5 to 10 000 µm**
Temperature range	**-150 to 600°C**
Heating rate	**0.1 to 20°C/min**
Cooling rate	**0.1 to 10°C/min**
Isothermal Stability	**±0.1°C**
Time/Temperature superposition	**Yes**
RH control	**optional**

Table 3-5: Main properties of the DMA system

A typical stress-strain curve of a pseudo-elastic NiTi wire is shown in Fig. 3-12. As shown in Fig. 3.12a, the strain corresponds to number 1 indicates the initial of the plateau and the one corresponds to number 2 is the end of the plateau. It is noteworthy to mention that the martensite is induced between these two points by the force applied: this is the SIM. The average stress value between points 1 and 2 is the plateau stress. The stress and strain of point 3 indicate the mechanical condition above the pseudo-elasticity and below the failure of the wire. The reverse transformation happens between points number 4 and 5. Moreover, the residual strain corresponds to point 6. The difference between the stress value of plateau and the reverse transformation is shown by number 7 and it is called as hysteresis width.

In a tensile curve at the beginning of the plateau, the corresponding value of effort (σ_{Ms}) and deformation (ε_{Ms}) are identified. In the same manner, the deformation at the end of the plateau (ε_{Mf}) and the deformation corresponding to the length of the plateau ($\varepsilon_{plateau}$) are calculated as the difference between deformation at the start and end of the plateau ($\varepsilon_{Ms} - \varepsilon_{Mf}$), as depicted in Fig. 3.12b.

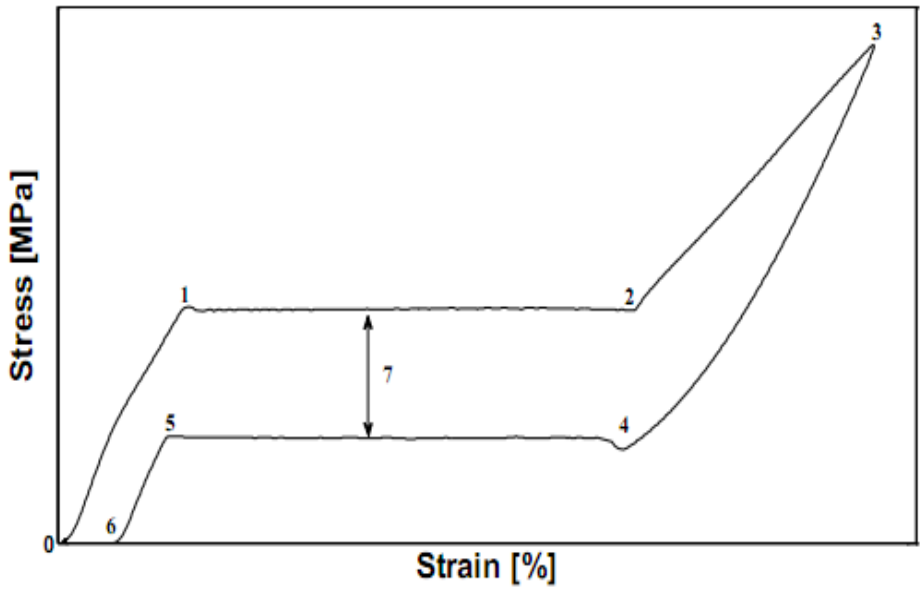

(a)

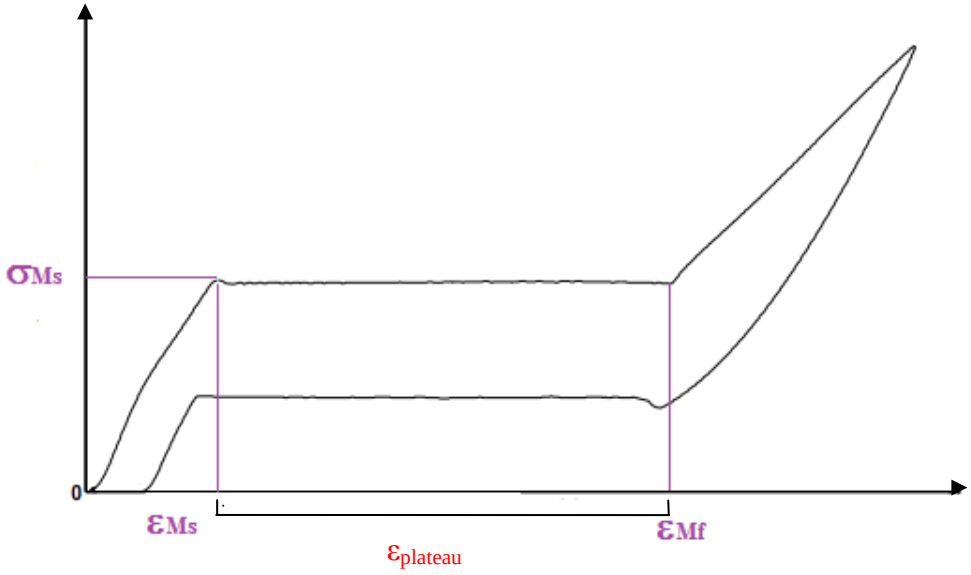

(b)

Fig. 3-12: Typical stress-strain of a pseudo-elastic NiTi wire in the austenitic state

3.5.3 X-Rays Diffraction Analysis

X-Rays Diffraction (XRD) is a characterization technique used for studying the microstructure of matter and for the determination of their structure.
X-ray diffractometer consists of three basic elements: an X-ray tube, a sample holder, and an X-ray detector. X-rays are generated in a cathode ray tube by heating a filament to produce electrons, accelerating the electrons toward a target by applying a voltage, and bombarding the target material with electrons. When electrons have sufficient energy to dislodge inner shell electrons of the target material, characteristic X-ray spectra are produced.
When the incident X-rays impinging the sample satisfies the Bragg Equation, constructive interference occurs and a peak in intensity occurs (see Fig. 3-13). A detector records and processes this X-ray signal and converts the signal to a count rate which is then output to a device such as a printer or computer monitor.
Peak positions occur where the X-ray beam has been diffracted by the crystal lattice. The unique set of d-spacings derived from this patter can be used to 'fingerprint' the mineral.
The geometry of an X-ray diffractometer is such that the sample rotates in the path of the collimated X-ray beam at an angle θ while the X-ray detector is mounted on an arm to collect the diffracted X-rays and rotates at an angle of 2θ. The instrument used to maintain the angle and rotate the sample is termed a "goniometer".

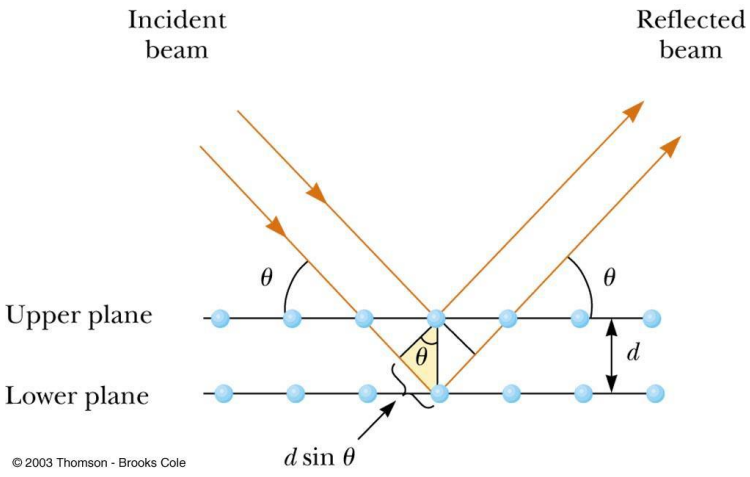

Fig. 3-13: Schematic of the XRD test

In this work the XRD analysis was done at room temperature on different samples: straight annealed, cold worked and the samples laser annealed at 50 mm/s in function of the laser power.
The XRD analysis was performed with higher resolution by using synchrotron light, in Elettra (Trieste). The facility of Elettra, depicted in the schematic of Fig. 3-14, allows to use high energy X-Rays for fine analysis of the wire structure. The main advantage, with respect to the previous XRD equipment, is the higher resolution of the spectrum acquired, which means to increase the precision of the pattern to be analyzed; this is very important when the width and the intensity of the peaks are correlated to the size of the crystalline structure, like the material texture.
In details, XRD patterns were collected in Debye-Scherrer geometry in transmission at the MCX instrument of the MCX beamline of Elettra at an incident wavelength of 0.6885 Å.
The samples, 20 mm in length, were placed into a quartz capillary (diameter size of approximately 200 μm), mounted on a goniometric head and spun during data acquisition. Patterns were recorded in the 10 to 55 ° 2theta range to access most of the main reflections.
Due to the high energy of the X-Rays, samples of 25 mm in length were put in rotation and the measurement was done in transmission mode.

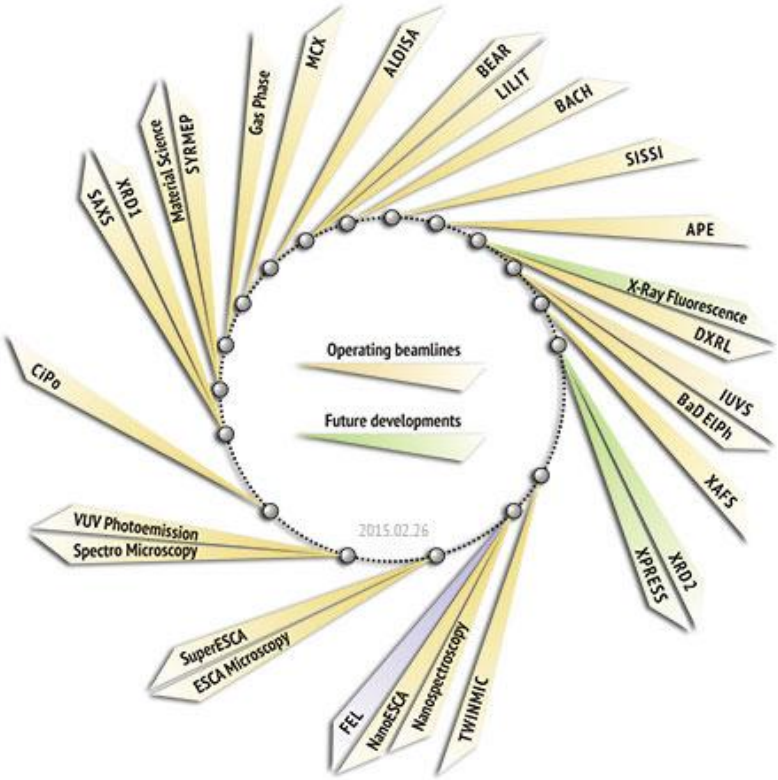

Fig. 3-14: Schematic of the beam lines structure of the Electra light synchrotron

Chapter 4

4 Analysis of results and discussion

In this chapter the results obtained from this research have been reported and their analysis were presented.
First the definition of the feasibility area of the main process parameters investigated was set; then, the effect of the process parameters in the entire feasibility window was correlated to the functional properties of the wires.

4.1 Definition of the feasibility area of the process parameters

The laser annealing was studied by changing the process speed and the incident power. The state of the wire which was subjected to the laser process was the cold worked condition, which was not associated to any phase transformations.
While three value of process speed were investigated, the minimum and maximum value of power, function of the process speed investigated, were variable. In fact, fixed a process speed, there was a value of power not able to induce the MT and even another value able to melt the wire. This study was performed in the range of power inside the values previously indicated.

Table 4-1 shows the power values associated with each process speed and the type of effect observed on the NiTinol wire, as a qualitative result of the DSC measurements.

V[mm/s]	P[%]	P[W]	material condition

50	35	45	no transformation
50	37.5	55	transformation
50	40	65	transformation
50	42.5	75	transformation
50	45	85	transformation
50	47.5	95	transformation
50	50	105	transformation
50	52.5	115	transformation
50	55	125	melting
65	37.5	55	no transformation
65	40	65	transformation
65	42.5	75	transformation
65	45	85	transformation
65	47.5	95	transformation
65	50	105	transformation
65	52.5	115	transformation
65	55	125	transformation
65	57.5	135	melting
80	40	65	no transformation
80	42.5	75	no transformation
80	45	85	transformation
80	47.5	95	transformation
80	50	105	transformation
80	52.5	115	transformation
80	55	125	transformation
80	57.5	135	transformation
80	60	145	melting

Table 4-1: relationship between power value in [%] and the values in [w] and effect of power on the material in relation to the speed of process

The combinations among the process speed and the power, which are able to induce the MT in the wire, are reported in Table 4.2 and shown in Fig 4.1.

V[mm/s]	Range p [%]	Δp	range p [W]	Δp	amplitude range
50	37.5-52.5	2.5	55-115	10	7
65	40-55	2.5	65-125	10	7
80	45-57.5	2.5	85-135	10	6

Table 4-2: numerical parameters for detecting the working area for each treatment condition

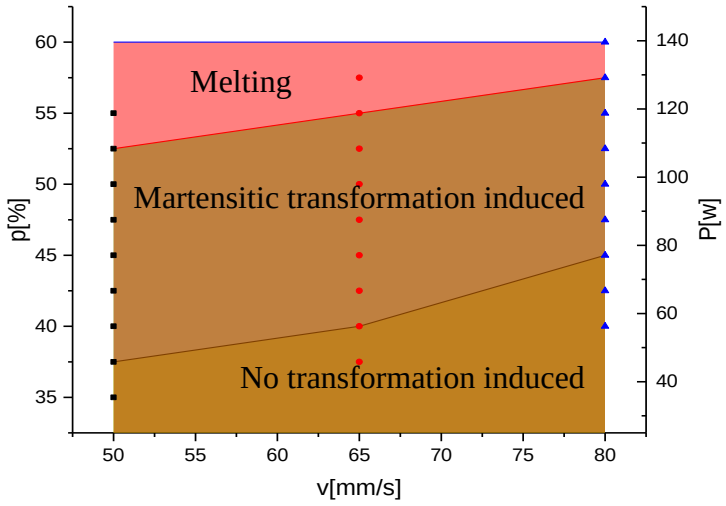

Fig. 4-1: Definition of the feasibility area for inducing the MT in the Nitinol wires

The analysis of working field (shown in Fig. 4-1) carried on three process speed is sufficient to provide information on the area of heat treatment developing (the middle part of the graph in Fig. 4-1). Therefore, for a process speed higher than that area we have to go upward and so it is necessary to employ higher power values in order to ensure the effectiveness of heat treatment at the same way, a lower process speed will lead to an area processing downward and consequently, decrease in power range is necessary to stay in effective area of heat treatment.

A clarification of the laser power emitted from the laser source is obtained by identifying the power emitted by the system, the power incident on the wire and the power actually absorbed by the material being processed.
The treatment is performed in a manner already described in schematic Fig. 3-6. Therefore in the heat treatment of the SMA wire only a part of the laser beam emitted from the laser source affects the upper part of the wire (Fig. 4-2) And the surface of the wire is affected by the central part of laser radiation.

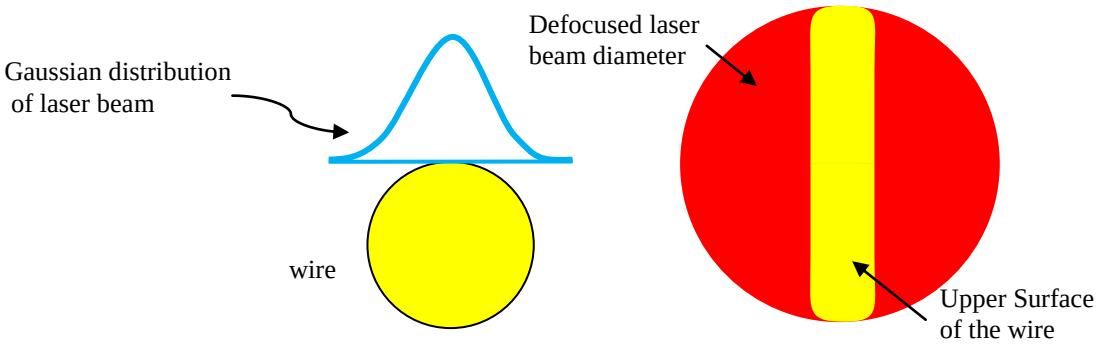

Fig. 4-2: representation of laser beam incident on the SMA wire during the treatment

4.2 Calorimetric analysis

The study of the calorimetric response of the wires, realized under different conditions, was performed in order to identify the shape of the DSC curves, which are associated to the MT.

4.2.1 Calorimetric analysis: straight annealed and cold worked wires

Fig. 4.2 shows the DSC scan of the commercially available wires in the straight annealed and in the cold worked conditions respectively. The straight annealed wire shows the peaks of the MT upon heating and cooling (see Fig. 4.2a), according to the conventional thermal treatment performed by the producer. The parameters of this conventional shape setting are not known; the information important for this work is the final calorimetric response of the material, which is considered as a reference of the wire to be used for biomedical applications.
Table 4.1 reports the characteristic temperatures of the MT and the corresponding heats exchanged, measured from the DC scan of the straight annealed wire.

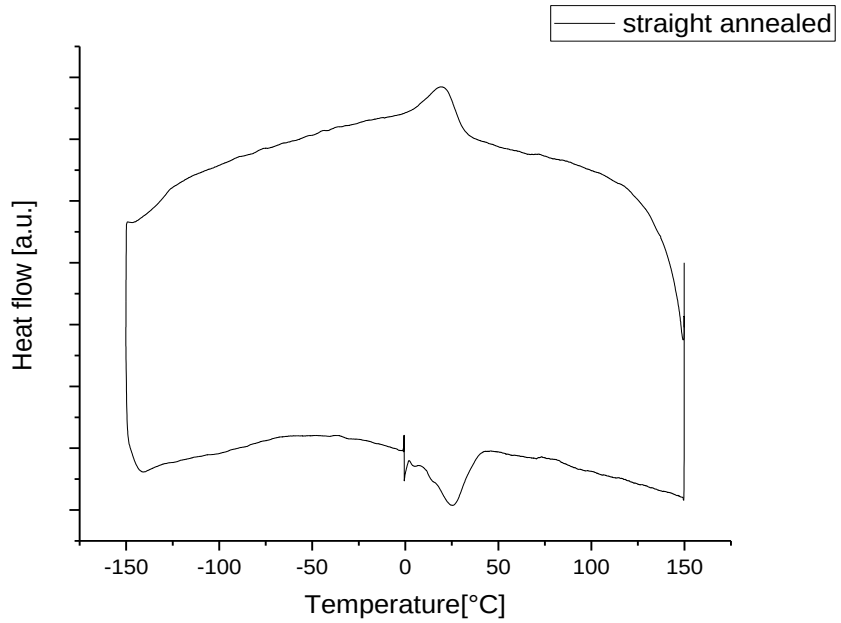

(a)

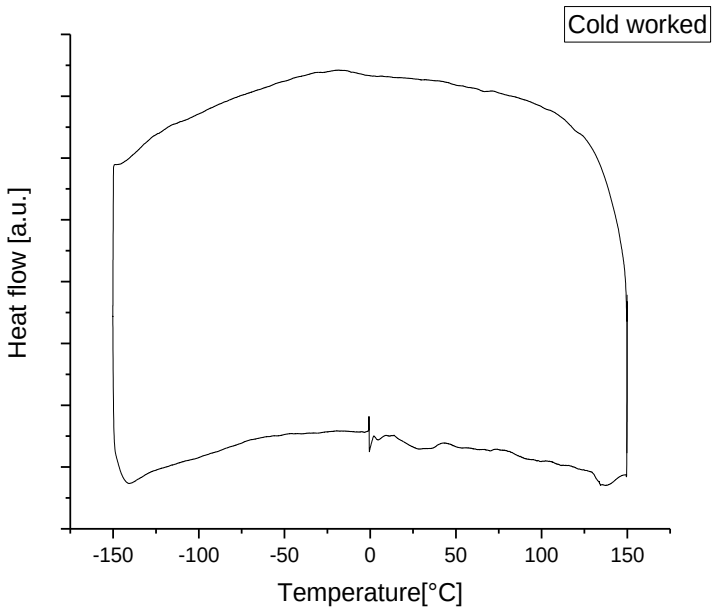

(b)

Fig. 4-3: DSC scans of the wires: straight annealed (a) and cold worked (b)

Ms [°C]	Mf [°C]	Hcool [J/g]	As [°C]	Af [°C]	Hheat [J/g]
32.4	-1.1	3.2	4.4	39.3	4.4

Table 4.1: Characteristic temperatures and heats exchanged of the straight annealed NiTinol wire

On the contrary, due to the severe degree of plastic deformation induced during the last step of cold drawing to the wire, the cold worked wire cannot show evidently the peaks associated to the MT, as depicted from Fig. 4-3.b.
This is the initial material state, which is required to perform the laser shape setting.

4.2.2 Calorimetric analysis: laser annealing

The laser shape setting has been performed on the wires, characterized by the cold worked condition (see Fig. 4-3.b). Fig. 4-4 shows the evolution of the MT, induced by the laser beam, during the shape setting performed at 50 mm/s as process speed.
In the lowest power value (35%) no peaks are observable. In comparison with cold worked wire (see Fig. 4-3.b), we can see the same calorimetric response as no phase transformation occurs under this process condition. The reason is that not sufficient energy was introduced by the laser beam for inducing the MT. In the next power step (37.5%) the transformation is present as a wide peak with low intensity upon heating and cooling.
Raising the power level (40%), the peaks of the MT are more evident. In the cooling, the peak is still wide but the transformation temperatures become more defined because the peak is sharper. By increasing the laser power, the temperature induced in the wire is increasing, too, and the functional properties of the wire can be evidently modified. Upon heating the transformation peak is also wide and jagged shape.
By increasing the power level up to 42.5%, in heating the peak of transformation from austenite to rhombohedric (R) is appeared before martensitic (M) peak; this peak is very wide and close to the M peak. On the other hand, upon heating the peak of reverse transformation got more intense, because a higher amount of phase change is involved in the MT. By increasing the power level up to 45%, the R peak gets very close to M peak, almost partially overlapped. On the contrary, the peak of the direct MT upon cooling and of the reverse MT upon heating appear very intense and well defined. With a power level higher (47.5%) in cooling phase, there had been a further rapprochement on the temperature range between the peaks of R and M, which are not distinct from one another. in this case R phase finish temperature and M start temperature cannot be determined separately but they are partially overlapped.

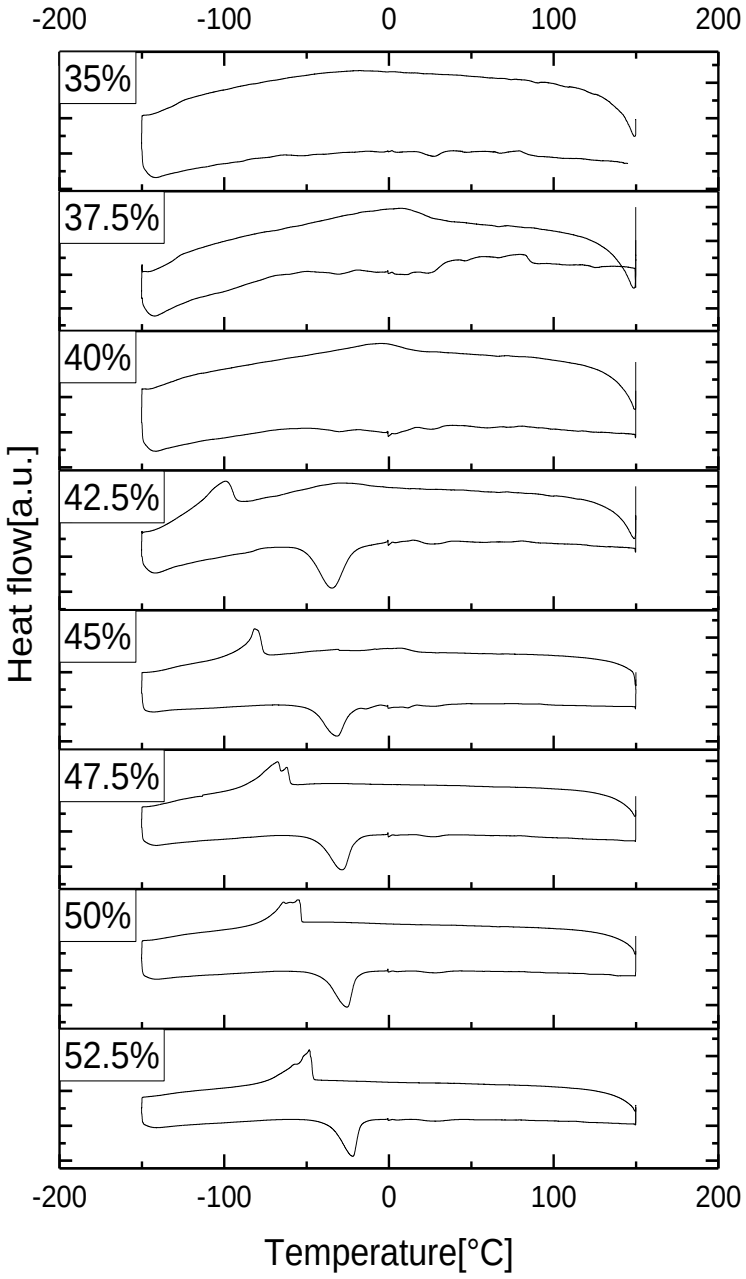

Fig. 4-4: Evolution of the MT in the wires, laser annealed, as function of the power at 50 mm/s process speed

Upon heating the austenite peak is well defined and intense, as in the previous case. This DSC signal may be associated to a state of the material which was subjected to a solubilization thermal treatment at high temperature.
The next power level (50%) shows a jagged shape peak in cooling due to continuity between R and M peaks. This kind of peak shape shows the probable formation of different phases that transform at distinct temperature. The last power value before melting of the material (52.5%) has the most intense peak in the cooling. From the lowest to the highest power, in the cooling phase, a narrowing of peak M occurs, until reaching the value of maximum temperature below the melting of the material.
Fig. 4-5 shows the trend of the phase transformation temperatures and the relative enthalpies in function of the power increase, fixed the process speed to 50 mm/s.
The quantitative analysis shows that upon cooling (see Fig. 4-5.a) the R-phase is not present for the entire power range investigated. Just in two middle power levels (42.5% and 45%) we can see the presence of the R phase, beyond and upper this power range the R-phase is not distinguishable since it is united with the M phase.
By increasing the power, the phase M first moves sharply toward lower temperature and then increases slightly. The similar occurs for the austenite (A) phase upon heating, as shown in Fig. 4-5.b. Upon heating the R phase is not visible from the DSC scan, but it is surely present.
A similar analysis can be done for the trend of the enthalpy. In cooling, at lower power value can be detected, as the peaks are very wide and not well defined and the amount of material involved in the MT is quite low.
With the increase of the power, the enthalpy increases slightly. In details, upon heating (Fig. 4-5.b) we can see a sharp increase at first, then for one power step a small decrease, and again increase.
In the following, the DSC results of the wires, laser annealed at higher levels of process speed, are reported.
Fig. 4-6 shows the DSC curves of the wires laser annealed at process speed of 65 mm/s at varying the power. The evolution of the MT is quite similar to previous one obtained.

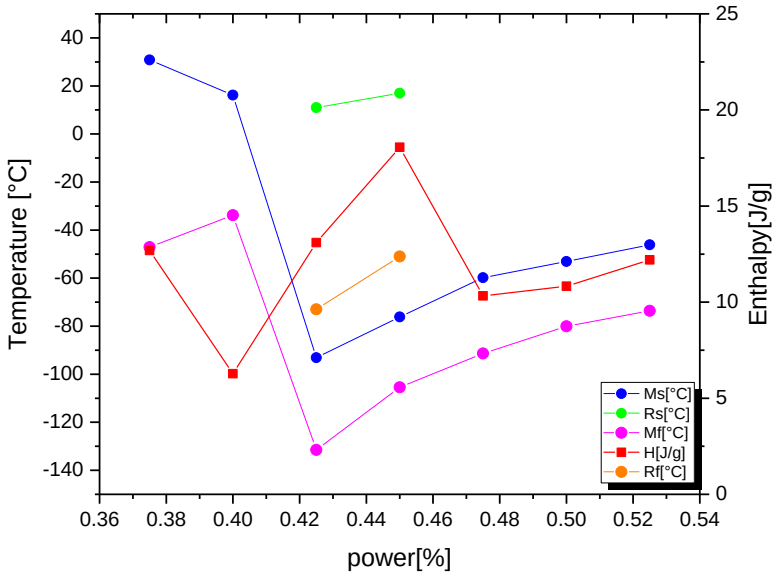

(a)

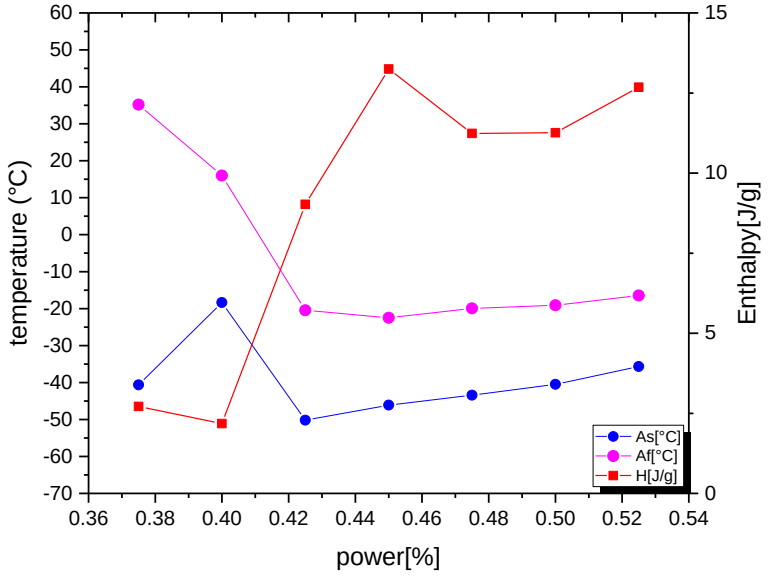

(b)

Fig. 4-5: Evolution of the characteristic features of the DSC scan of the wires, laser treated at 50 mm/s at varying the power: cooling (a) and heating (b)

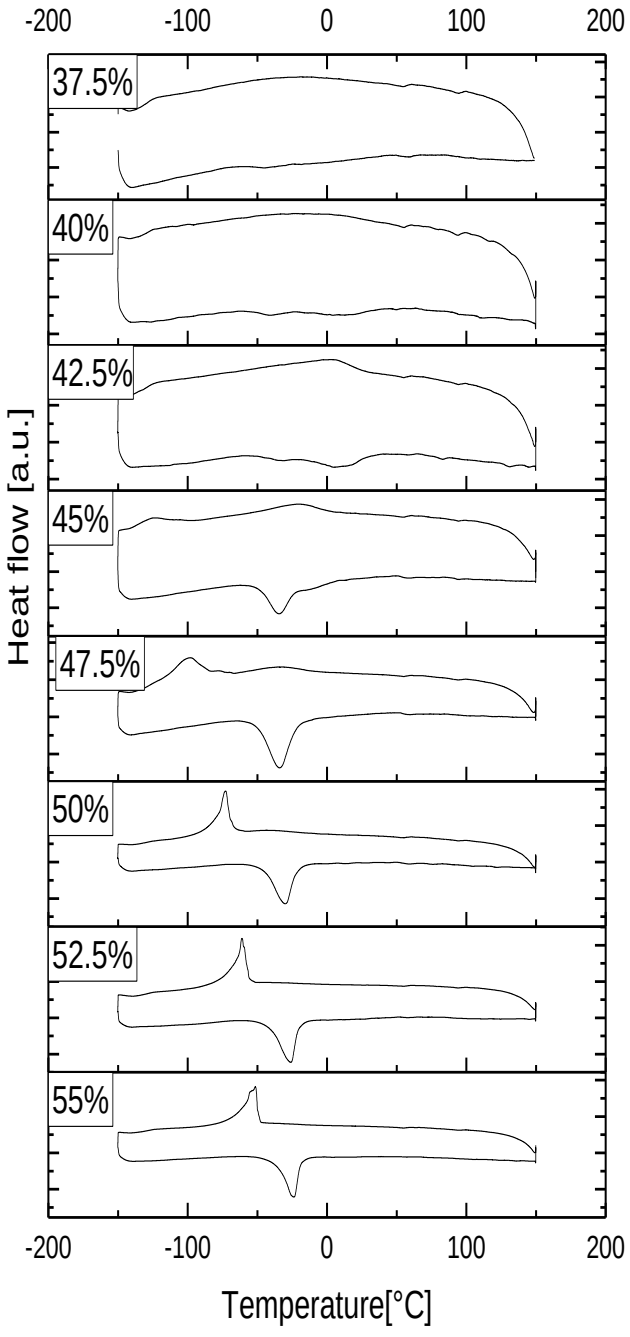

Fig. 4-6: Evolution of the MT in the wires, laser annealed, as function of the power at 65 mm/s process speed

The lowest values of power, such as 37.5% and 40%, are not able to induce any phase transformation both upon cooling and heating. By increasing the power up to 40%, the R peak is very wide but identifiable upon cooling while the M peak cannot be detected. Upon heating a wide and blunt peak is observable; only at higher magnification of the DSC curve, two peaks may be seen upon heating. By increasing the power up to 42.5%, the shape of the peaks and their position along the temperature axis almost remain similar to the previous case but they got a little more intense, due to the higher energy given by the laser beam. Another increase of the power level up to 45%, in the cooling phase the first peak, which comes into appear is R phase transformation following by the M peak, are quite visible but wide and blunt. On the contrary, upon heating the A peak is intense and well defined.

In the following step of power (47.5%), the peak of M phase tends to approach the one of the R phase. The intensity of M peak in cooling and a peak in heating grows, because of the increase of the temperature induced in the wire. All the peaks are well defined in this process condition, which can indicate a successful annealing. The three power levels before melting are associated to high intensity peaks both upon cooling and heating. In these three cases the R peak is not visible from the DSC curve. Moreover, with increasing the power the M peak moves to lower temperature and the A peak becomes sharper. This happens when the NiTinol is subjected to high temperature thermal treatments, in which the solubilization of the microstructure occurs.

This modification of the shape of the transformation peaks is due to a change of the microstructure: large peaks indicate a high degree of defects in the crystalline grating, which are mostly dislocations. On the contrary, sharp and high intensity peaks can be obtained from high temperature thermal treatments and they are associated to the removal of the previous defects. As a consequence, the material is characterized by low density of dislocations and so it becomes softer [16].

Fig. 4-7 reports the trend of transformation temperatures and of the corresponding enthalpies as a function the of laser power.

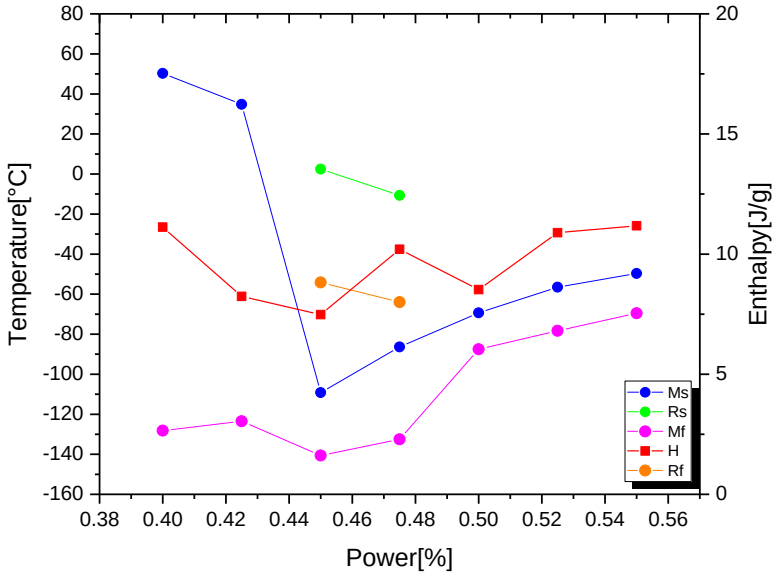

(a)

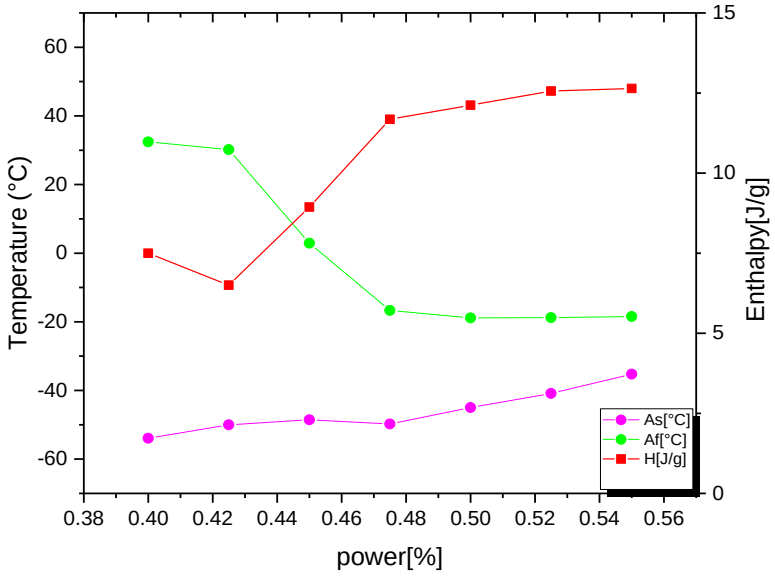

(b)

Fig. 4-7: Evolution of the characteristic features of the DSC scan of the wires, laser treated at 65 mm/s at varying the power: cooling (a) and heating (b)

In the intermediate value of process speed (V=65mm/s), a similar evolution of the MT has been detected by increasing the laser power. As previously observed, we can see the presence of the R-phase during the cooling of the DSC only for two power values but it has one step shift to higher power values.
The M phase during cooling is characterized by a low temperature range; then, with increasing the power it shifts to higher temperature, approaching to the R-phase and it increases very slightly at higher power values.
During the heating, the A phase does not change significantly its characteristic temperatures.
The enthalpy is evidently growing upon heating from 6 J/g up to 12 J/g with the increase of the power; on the contrary, the enthalpy does not evidently change upon cooling with the increase of the power and it remains in the range from 7 J/g up to 12 J/g.
With increasing process speed up the highest value investigated in this work, up to 80 mm/s, the evolution of the DSC response in function of the power is shown in Fig. 4-8.

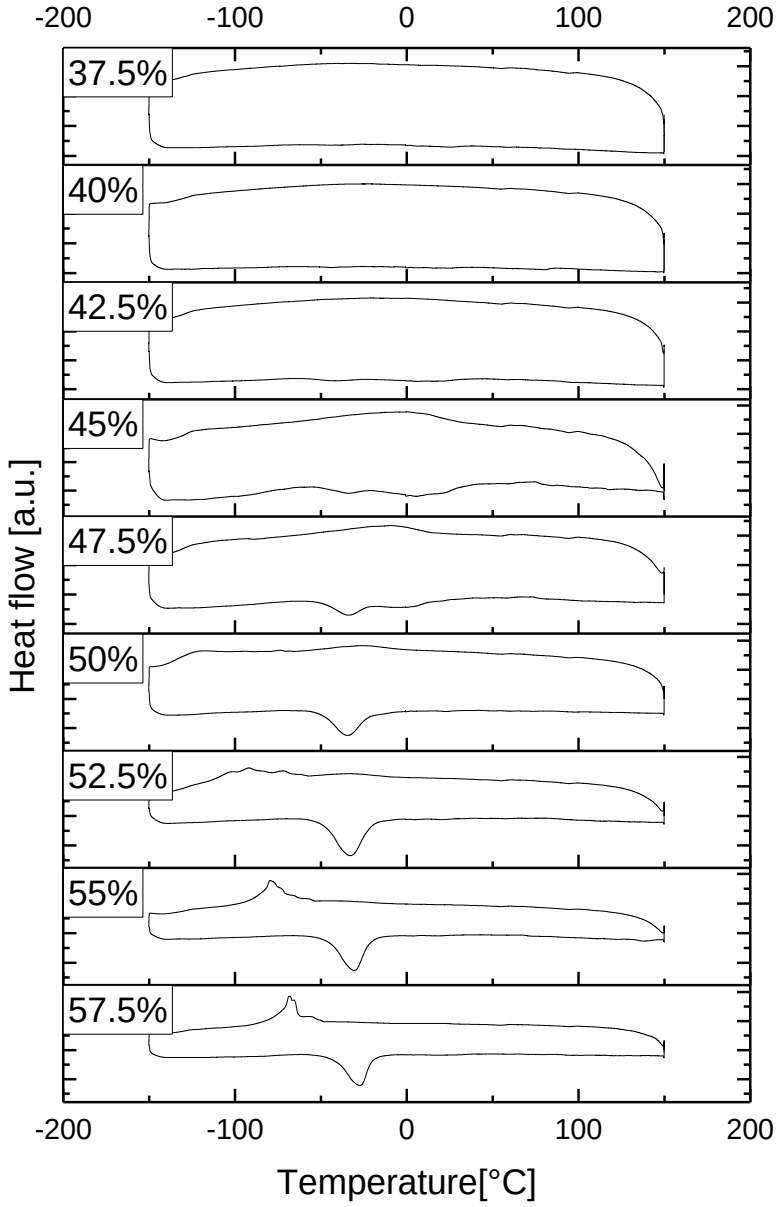

Fig. 4-8: : Evolution of the MT in the wires, laser annealed, as function of the power at 80mm/s process speed

The lowest value of power, equal to 37.5%, shows no phase transformation induced as well as for the next power step (40%). By increasing the power up to 42.5%, the MT can be induced with a soft and very wide peaks. In the following steps of power (45%) the intensity of the M peak upon cooling increases but it is still wide: as well the width of the peak indicates that the material is in continues transformation over a wide temperature range, consequently its homogeneity in the phase transformation is quite poor. The heating step of the thermal cycle instead is characterized with two small peaks, very close each other, which are due to the coexistence of R phase and a phase, in the same temperature range. Raising the power level up to 47.5%, upon heating the R peak and a peak are not distinct from one another but they are overlapped. The shape and the intensity of the M peak upon cooling doesn't change significantly. At higher power (50%) the cooling phase unlike previous cases of this speed, consist of two blunt peaks of R phase and M, which are very close together. The heating step, instead, is characterized by a single peak of A and more intense. A further increase in power (52,5%) shows, due to continuity between R and M peaks in cooling step, a jagged shape peak, as the result in the formation of different phases, transforming at distinct temperatures. The A peak during heating remains well defined and even more intense than the previous case. The last two step power values before the melting of the material indicate the most intense peaks in the phase of cooling and heating.(b)

Fig. 4-9 Shows the trend of the transformation temperatures and the corresponding enthalpies in function of the power increase, fixed the process speed to 80 mm/s.

From DSC analysis of the highest process speed treatment, we can see during cooling (see Fig. 4-9.a) phase R is present and recognizable only for one power condition (P=50%). Up to this power, the peak of M moves toward higher temperature.

The performance of the A phase during heating (see Fig. 4-9.b) shows the peak of A, that does not undergo to large displacement and it remains at a temperature interval ranging from -20°C down to -60°C. The R phase upon cooling is presented only for the two first power range.

Except one power condition, the enthalpy is growing in both cooling and heating stages with increasing the laser power.

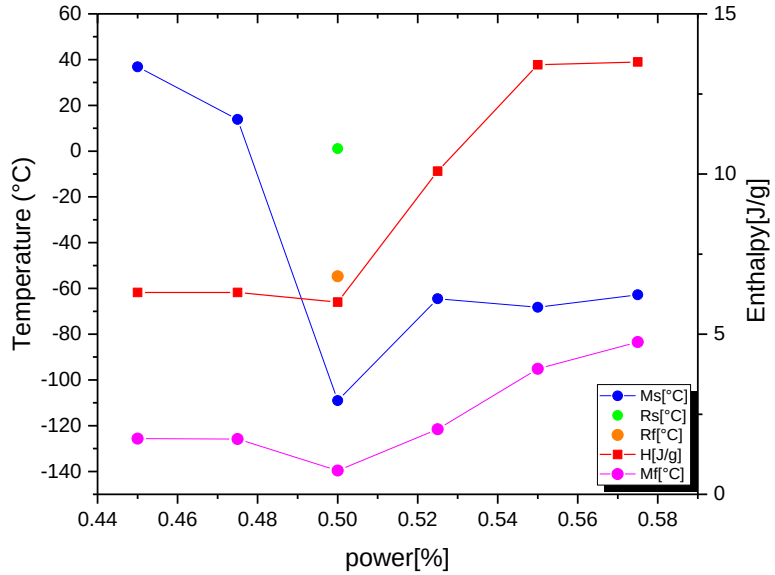

(a)

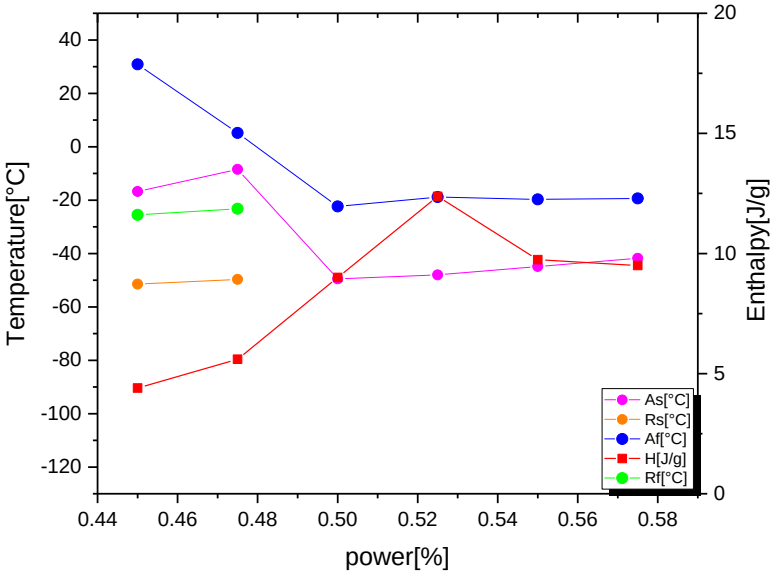

(b)

Fig. 4-9: Evolution of the characteristic features of the DSC scan of the wires, laser treated at 50 mm/s at varying the power: cooling (a) and heating (b)

4.3 Mechanical characterization

The mechanical tests were conducted to evaluate the stress-strain response for each process condition of the wires, both conventionally and unconventionally annealed.

4.3.1 Mechanical characterization: cold worked and straight annealed wires

Fig. 4.10 shows the stress-strain curve of the commercially available wires in the straight annealed and in the cold worked conditions respectively.
Fig. 4.10a shows the mechanical response of the cold worked wire: according to the previous DSC measurement, the wire without any annealing does not show the MT, so it can be only deformed with any possibility to show the pseudo-elasticity. Due to the high degree of plastic working, the wire is hardened and it is failed similarly as a brittle material.
On the contrary, the straight annealed wire shows a stress-strain hysteresis loop (see Fig. 4-10b), according to the conventional thermal treatment performed by the producer; it is visible the pseudo-elastic response, present at room temperature.
Table 4-3 reports the mechanical characteristic parameters of the straight annealed wire, which is the reference to be compared with the unconventional heat treated wires.

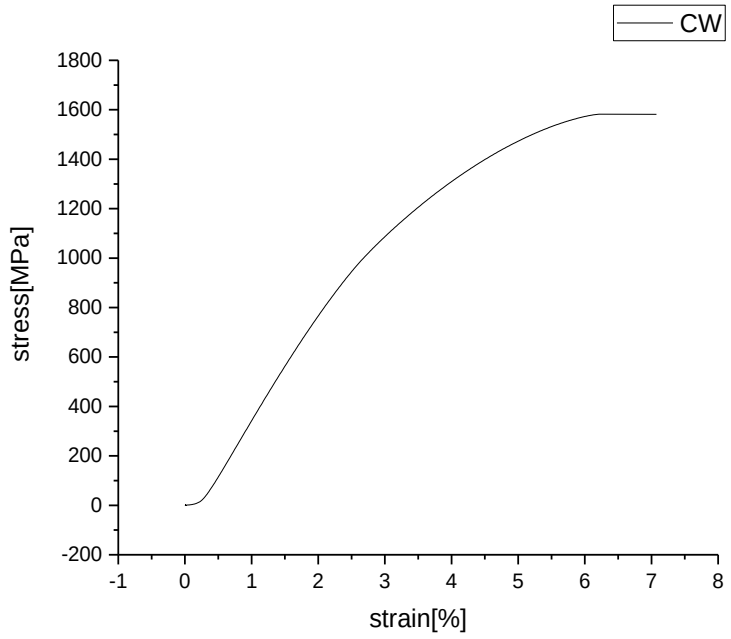

(a)

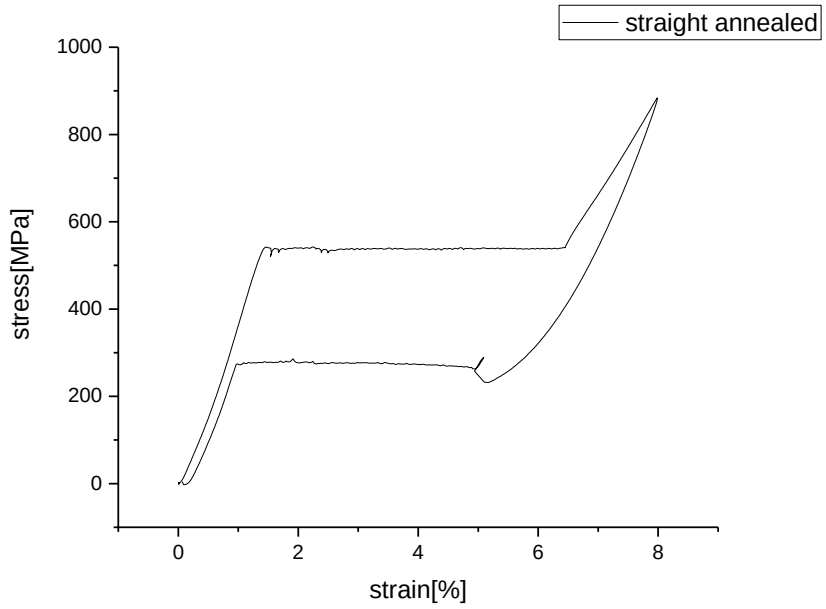

(b)

Fig. 4-10: Stress-strain curve of the wires: cold worked (a) and straight annealed (b)

Maximum stress [MPa]	Plateau stress [MPa]	Plateau start strain [MPa]	Plateau finish strain [MPa]	Residual strain [-]	Mechanical hysteresis [MPa]
1120	595	1.84	6.64	0.05	340

Table 4-4: Characteristic features of the pseudo-elastic behavior of the straight annealed wire, tested by 8% in strain

4.3.2 Mechanical characterization: laser annealed wires

The cold drawn NiTinol wires were heat treated by using the laser beam at different values of power and process speed. Fig. 4-11 shows the evolution of mechanical response over the entire range of laser power investigated, performed at 50 mm/s as process speed. All the test were performed up to 8% as final strain and then the wire unloaded in a close loop.
It can be seen from the Fig. 4-11 that the initial value of power 35% is not enough to induce the pseudo-elastic flag, characteristic of this material. Anyways, by increasing the power up to 37.5% the pseudo-elastic behavior is going to be shown, due to the increase of the temperature reached during the laser annealing: the material was softer and the deformation becomes easier. An increase of the power in the range 40%-42.5% shows the best pseudo-elastic response in terms of length of the plateau as well as in terms of negligible residual strain. This response is very similar to the one given by the straight annealed wire.
Under further increasing of the power, the plateau in the stress-strain curve is going to disappear and material doesn't show the pseudo-elastic behavior anymore. In fact, the temperatures of the thermal treatment are too much high and so the solubilization of the material occurs, causing a large effect of softening.

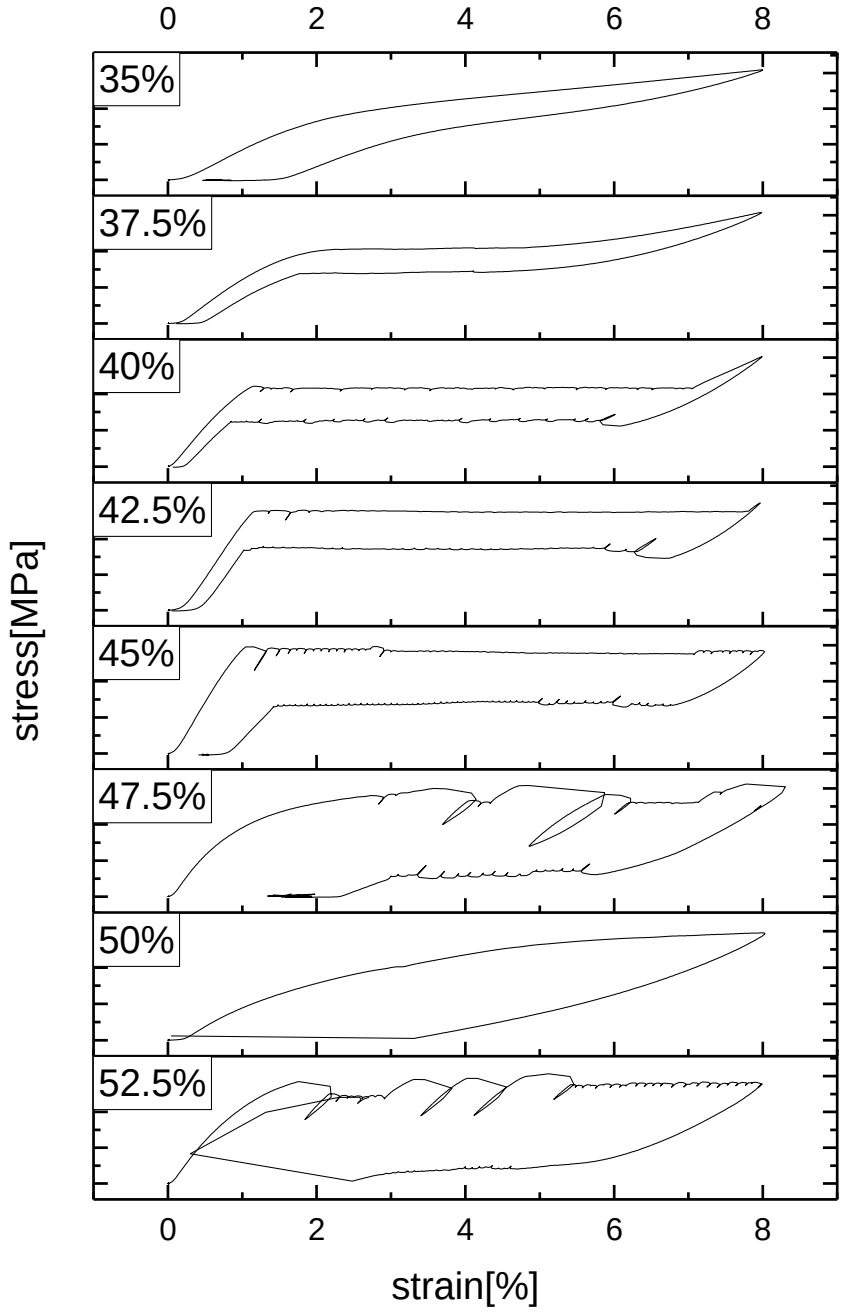

Fig. 4-11: Stress-strain curves of the laser annealed wires, realized at 50 mm/s at varying the power

Fig. 4-12 shows the trend of variables, which were measured for the characterization of the stress-strain curve of the laser annealed wires at 50 mm/s.

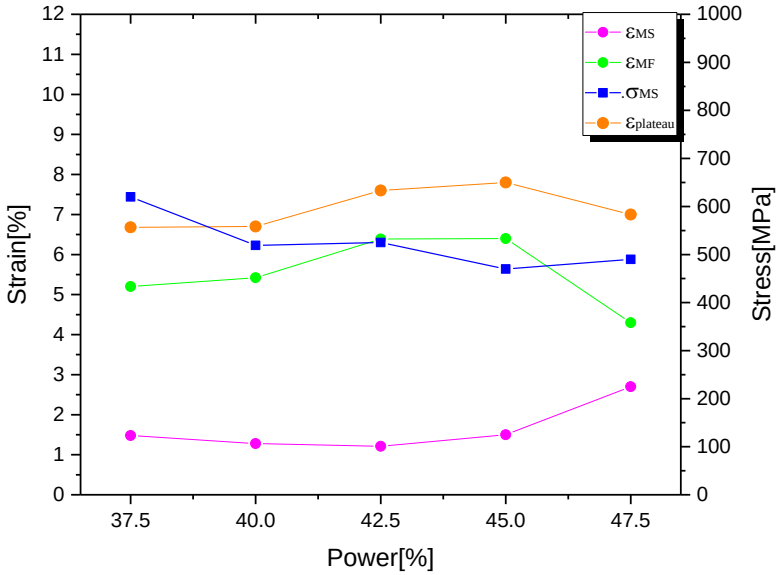

Fig. 4-12: Evolution of the characteristic features of the stress-strain curve of the wires, laser treated at 50 mm/s at varying the power

As it is observed in Fig. 4-12, upon increasing the power from 37.5% up to 45%, the ε_{Ms} almost remains constant at a value of 1.5% and it increases only at 47.5% up to 2.5%.
Both ε_{Mf} and $\varepsilon_{plateau}$ increase from 5% and 6.5% up to 6% and 7.5% respectively with the same slop when the power increases from 37.5% up to 45%. The stress of the plateau $\sigma_{plateau}$ decreases slightly from 600 MPa to 500 Mpa: the main reason can be due to the softening, occurring in the material treated at increasing temperatures.
Similarly to the previous conditions, in the following the stress-strain curves of the wires, laser annealed at higher process speed, are reported.
Fig. 4-13 shows the stress-strain curves of the wires laser annealed at process speed of 65 mm/s at varying the power.

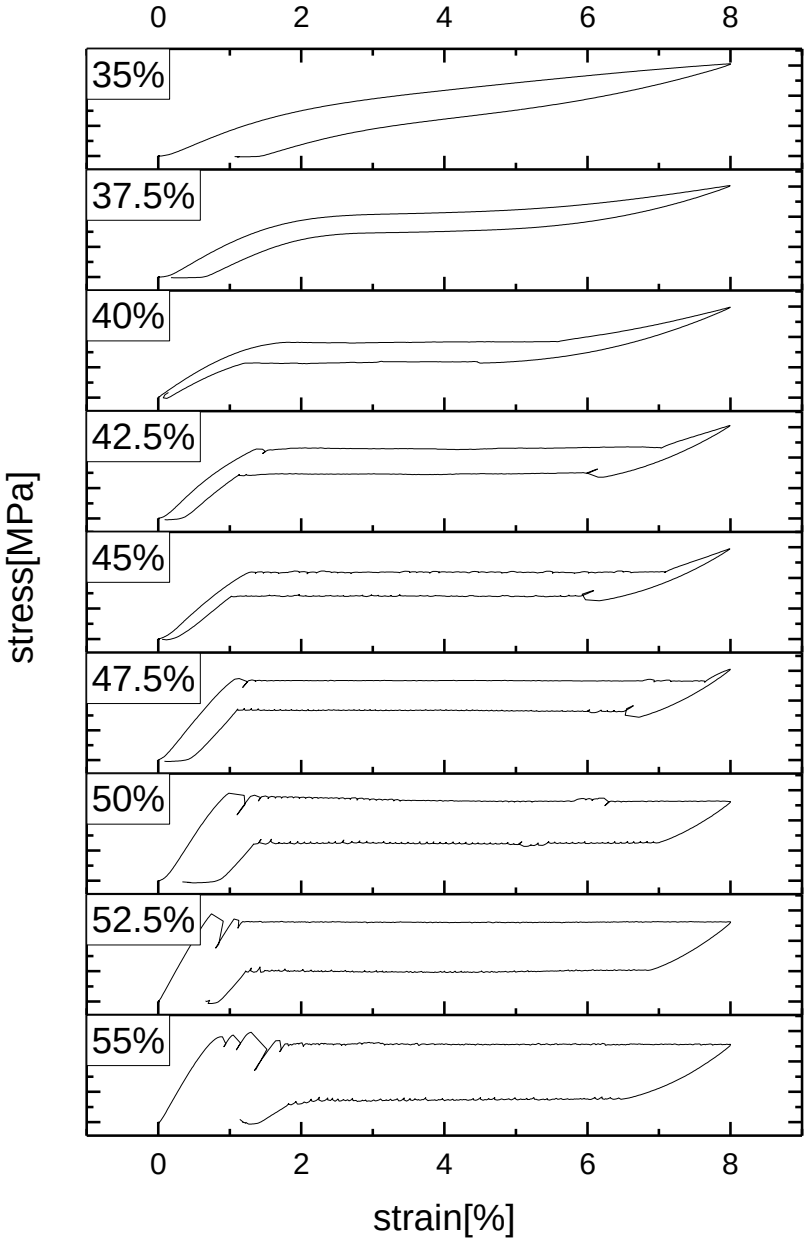

Fig. 4-13: Stress-strain curves of the laser annealed wires, realized at 65 mm/s at varying the power

The first level of power 35% cannot induce the MT and so the pseudo-elastic response in the Nitinol wire; in fact, no pseudo-elastic flag can be seen. By increasing the power, as observed in the previous evolution of power, the pseudo-elastic behavior starts to be manifested; a larger range of power at 65 mm/s can be associated to the possibility of the laser process to induce the pseudo-elasticity. By increasing the power, even if the pseudo-elasticity remains, the mechanical hysteresis increases.

From the Fig. 4-14 it can be seen that ε_{Ms} remains almost constant and it values in the range from 1.5% to 2% with increasing the laser power. In opposition, ε_{Mf} and $\varepsilon_{plateau}$ increase with a trend similar to the previous case while $\sigma_{plateau}$ decreases from 800 MPa down to 450 MPa.

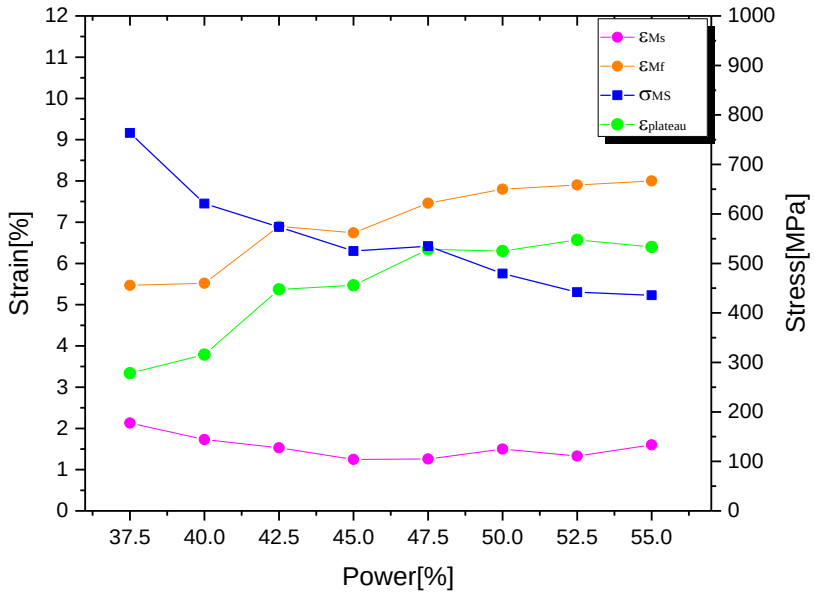

Fig. 4-14: Evolution of the characteristic features of the stress-strain curve of the wires, laser treated at 65 mm/s at varying the power

With increasing the process speed from 65 mm/s up to 80 mm/s, a similar trend of stress-strain behavior can be obtained, as shown in Fig. 4-15.

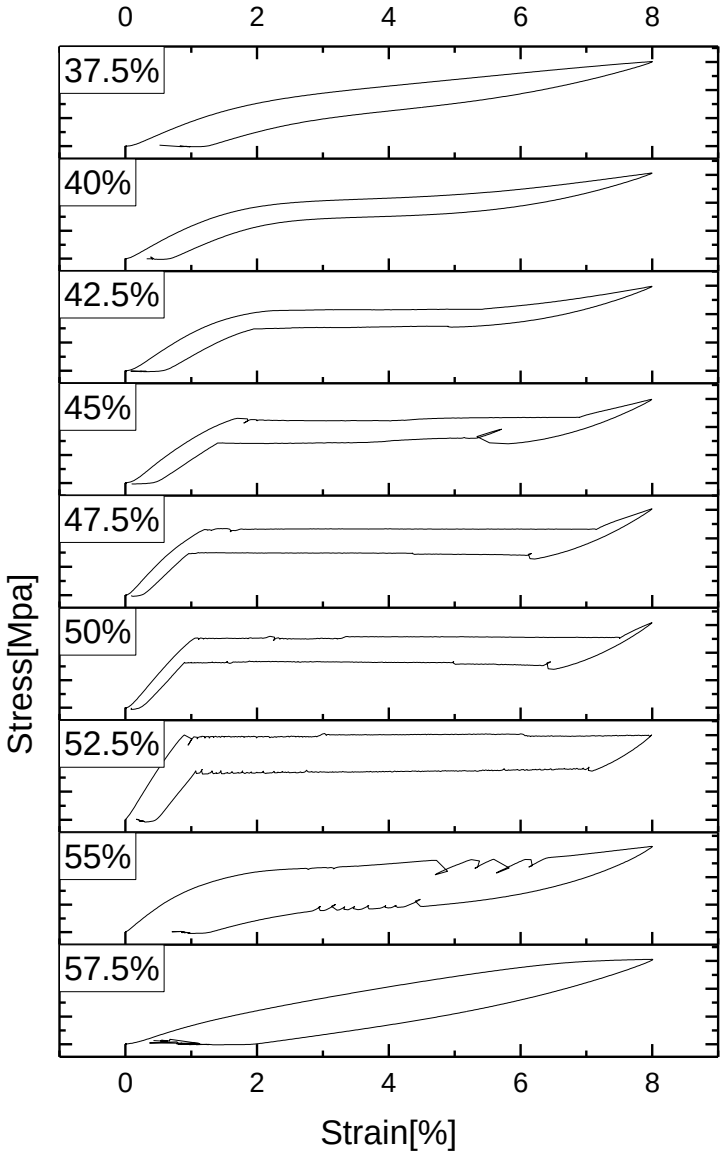

Fig. 4-15: Stress-strain curves of the laser annealed wires, realized at 80 mm/s at varying the power

At the lowest laser power no plateau is observable. It indicates that the power was not sufficient to induce MT in the material.
By increasing the laser treatment power from 37.5% to up 50% the pseudo-elasticity is induced and plateau length increases step by step. In opposition the residual strain is decreasing, due to the almost complete strain recovery at room temperature. Above these values, the material becomes soft and the plateau disappears: high temperature thermal treatment, done at high power of laser beam, contribute to the removal of the defects in the material. Therefore, the material becomes softer and with less dislocations, and can be recover more completely during unloading. In the case of the next laser beam power (52.5%), the maximum stress is equal to the stress of plateau; we can see the longest plateau in this laser power condition, but the residual strain is increased. Upon this laser treatment power, the plateau is decreasing and, on the contrary, the residual strain is growing. Increase in the residual strain means the reverse transformation from stress-induced martensite to parent phase is incomplete, since a part of martensite remains below this reverse transformation finishing temperature [40]. In the highest power value before melting the material, the martensitic transformation plateau disappears.
Fig. 4-16 shows the trend of the characteristic features of the SMA stress-strain curve. At this process speed, the martensitic plateau only appears on the power condition in the range from 42.5% up to 55%. Same as the previous condition, the material is not able to show plateau at too high temperatures. It looks that the deformation at the beginning of the plateau decreases from about 2% to 0.8%, as the laser power increases from 42.5% to 52.5%. On the contrary, ε_{Mf} and $\varepsilon_{plateau}$ grow with increasing the power. The amount of this change is from about 5% to 8% and 3.5% to 7% for ε_{Mf} and $\varepsilon_{plateau}$ respectively. This increase can show elongation of plateau during this power range.

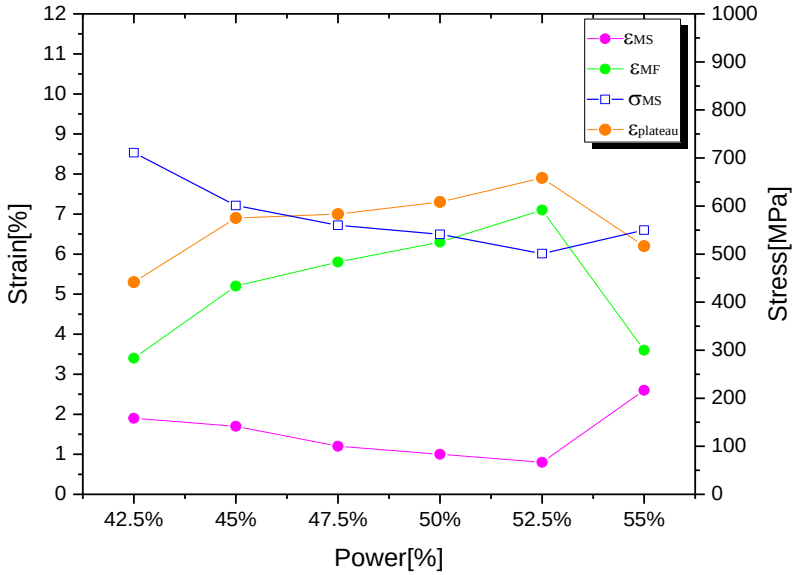

Fig. 4-16: Evolution of the characteristic features of the stress-strain curve of the wires, laser treated at 80 mm/s at varying the power

4.4 Analysis XRD by using Syncrotone light

In this characterization the evolution of the characteristic peak of the austenite phase was studied in function of the power of the laser beam, fixed the process speed equal to 50 mm/s. These results were compared to the ones of the straight annealed wire, realized by conventional shape setting, and of the cold worked wire.
The pattern collected on the sample, laser annealed at 40%, is shown in Fig. 4-17. The Miller indexes for each reflection are displayed on the top of each Bragg peak.

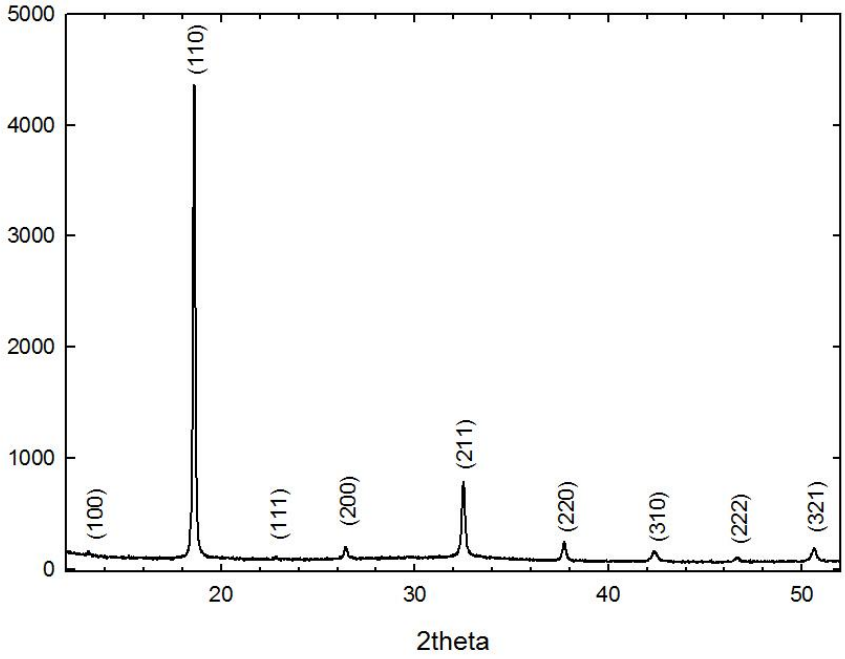

Fig. 4-17: Characteristic XRD pattern of the austenite in NiTinol

In Fig. 4-18 the comparison among the XRD spectra of the wires in different conditions is depicted. It can be observed that the cold worked sample shows large peaks, due to the high density of dislocations generated by the cold drawing. The two samples, conventionally and laser annealed, indeed show sharper peaks, because of the effect of the thermal treatment.

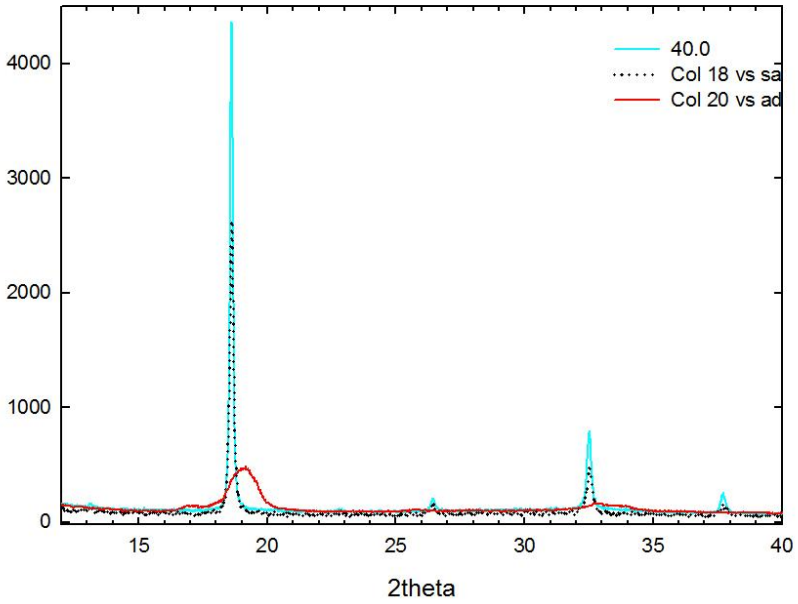

Fig. 4-18: XRD spectra of the wires in different conditions: cold worked, straight annealed and laser annealed at power of 40%

In Fig. 4-19 all the patterns of the wires, laser annealed by increasing the power from 32.5% up to 52.5%, are shown; in details, the peak of the austenite with (110) reflection was considered in this analysis, as it is the principal one. In addition Fig. 4-19 shows even the peak of the straight annealed wire, which has to be compared to the ones obtained by laser annealing.

All the samples show austenite as at least the main phase present. Some residual martensite seems to occur in the sample realized with the lowest power level (32.5%) while secondary phases are also evident in the sample realized with the highest power level (52.5%).

This is in good agreement with the previous DSC measurements; in fact, low power cannot induce the MT, which occurs usually below room temperature for the pseudo-elastic NiTinol, so this means that at room temperature residual martensite can be found. On the contrary, at high power, immediately below the melting of the wire, a solubilization occurs and the proper microstructure of the NiTinol is lost.

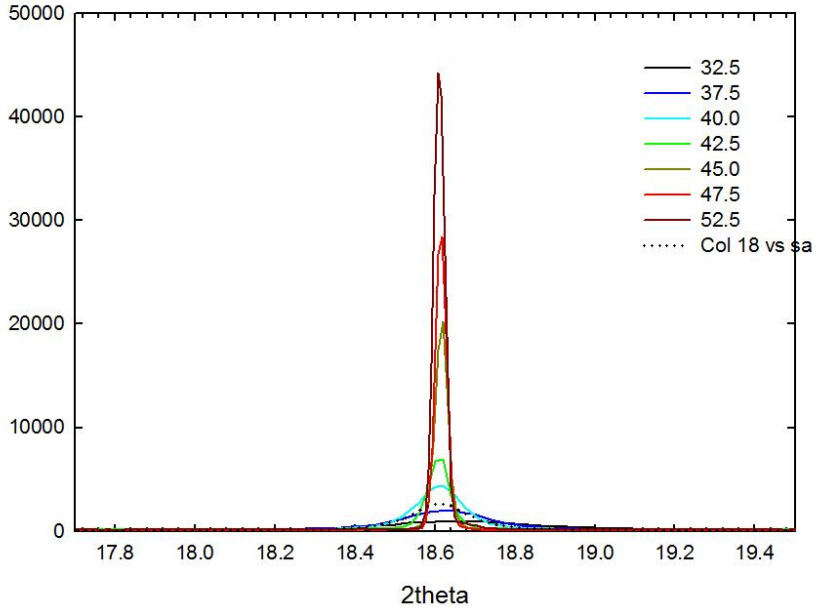

(a)

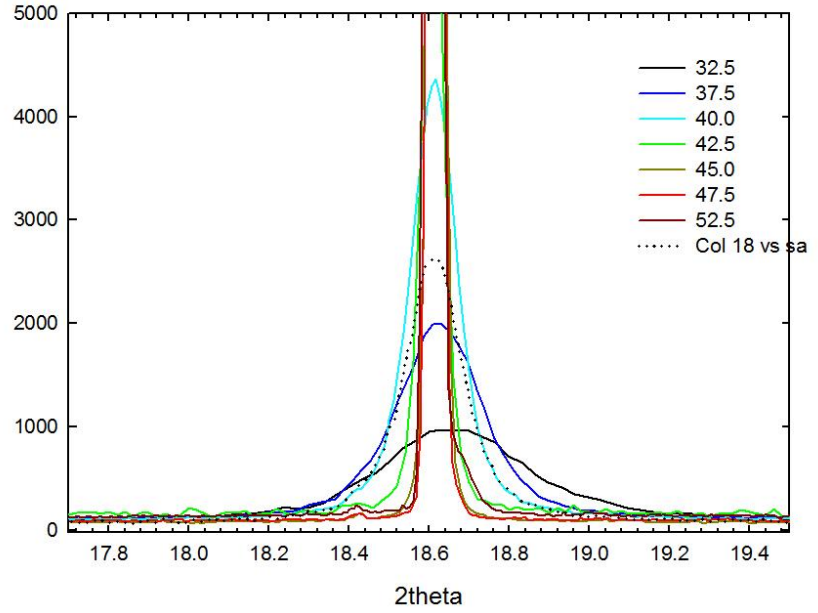

(b)

Fig. 4-19: Evolution of the main peak of the austenite by increasing the power: entire peak (a) and its magnification (b)

The different levels of power used during the laser annealing can affect the line profile of the experimental patterns: the higher the laser power, the sharper the diffraction peaks. The broadening of a diffraction peak is closely related to the density of extended defects (such as dislocations) of the corresponding crystallographic plane, as well as to finite size effects. The broadening is quantitatively defined by fitting the XRD peaks with Pseudo-Voigt functions (combination of a Gaussian and a Lorentzian function) and extracting the integral breadth, hereafter beta.

The trend of beta with the increase of the power of the laser beam is shown in the plots of Fig. 4-20. It is possible to observe that the effect of the power is very similar for different crystallographic planes; moreover, the broadening of the main peak analyzed, characteristic of the straight annealed sample, lies in between the values found for 37.5% and 40% laser power (see discontinuous line). Additionally, beta saturates for power higher than 45%, because the instrumental broadening due the instrument (see dot line) exceeds that arising from the sample.

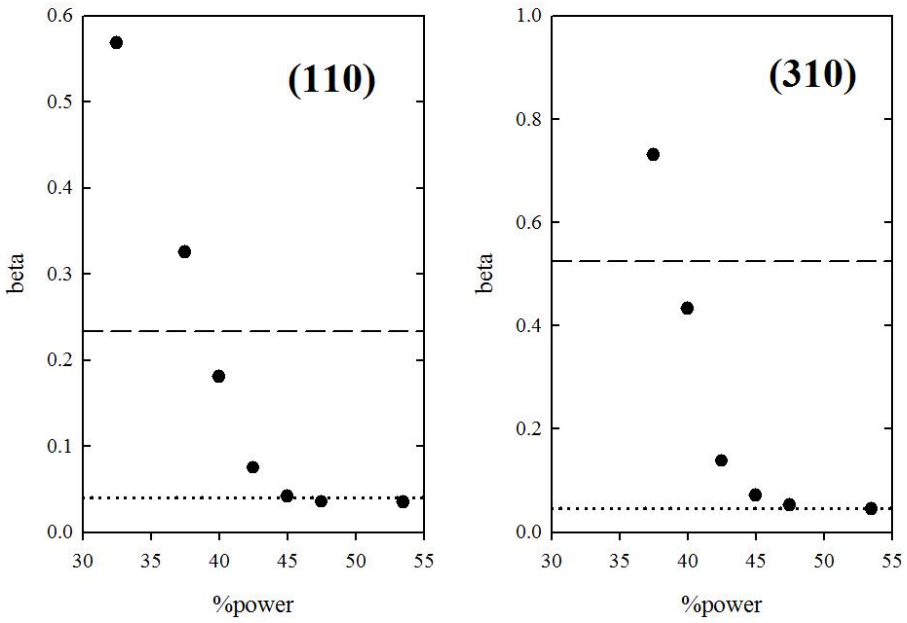

(a) (b)

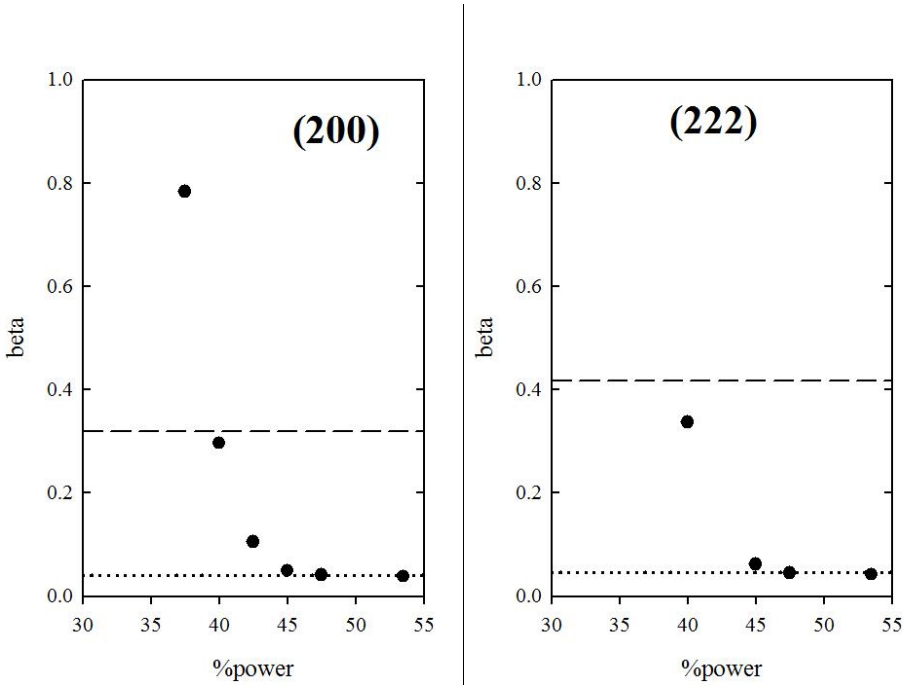

(c) (d)

Fig. 4-20: Evolution of beta of different orientations in function of the laser power: a (110); b (310); c (200) and d (222)

The laser power does not affect the line profile only, it rather slightly modifies the relative integrated intensity of the diffraction peaks. This effect is strictly related to the texture of the wire; in details, a possible explanation of this effect is that the laser annealing is performed faster than the conventional one, done in furnace, and it can induce a preferential microstructure modification along the wire length.

In fact, the laser treatment has been performed along the wire length, so it is reasonable to induce a preferential grain grow or any types of modifications along this direction, according to the mono directional heat conduction. On the contrary, the treatment in furnace is performed by introducing the heat in all the volume of the wire without any preferential direction.

The relative intensity of the peaks are shown in Fig. 4-21. The intensities are normalized to the reference value, as they would correspond to in the case of a perfect powder average, i.e. in the absence of textures. The cold drawing of the material modifies the natural intensity distribution and favors the (110) reflection with respect to the others.

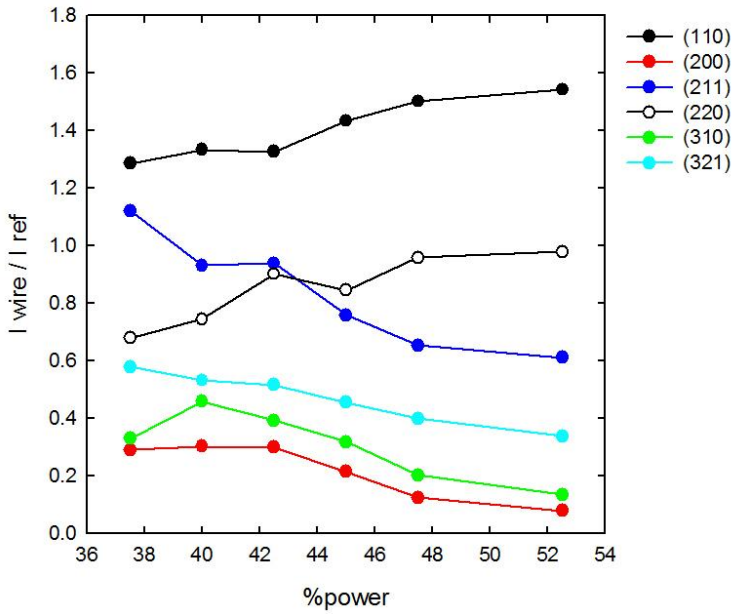

Fig. 4-21: Evolution of the relative peak intensity as function of the laser power

By monitoring the evolution of the relative intensity with the power of the laser it is possible to observe that the relative intensity of all reflections reduces but the intensity of the (110) reflection increases, adding a further texture contribution to that induced by wire drawing.

Chapter 5

5 Conclusions

In this thesis work an unconventional method for doing a fast thermal treatment of annealing, so called as shape setting, of NiTinol thin wires by using laser technology has been studied.
The experiments were performed on the cold worked wires with a diameter equal to 100 µm. The performances of the laser annealed wires were compared to the ones of the straight annealed wire, which can be found in the market.
This work led to the following conclusions, which are pointed out as follow:

- An experimental DoE was done for defining the feasibility area of the main process parameters, such as the laser power and the process speed.

- The laser annealing is able to induce the martensitic transformation in the cold worked wire, consequently it can determine the pseudo-elasticity in the NiTinol wires studied in this work.

- It is observed that the calorimetric behavior and the mechanical properties of the material is closely related to the combination of the process parameters and therefore to the amount of energy absorbed by heat treatment.

- For all the values of process speed investigated, it was found a laser power able to induce the functional properties of the wires at least similar or even better than the one offered by the straight annealed wire, commercially available in the market.

- The microstructure analysis indicates that a preferential orientation of the material texture can be induced by the laser annealing; this texture appears to be more orientated by the laser beam than the one obtained by the conventional annealing. This can be an explanation why the functional properties of the laser annealed wires are at least compatible to the ones of the straight annealed wires.

In conclusion we can say that in this thesis work it is demonstrated the capability of the laser technology to perform a heat treatment of annealing on thin wires of NiTinol for inducing the required functional properties.
Peculiar characteristics, such as high productivity but even possibility of performing localized annealing, allow laser annealing of thin wires of NiTinol to be considered as a potential alternative method for performing the shape setting process for industrial applications.

6 Bibliography

[1] X. K. Otsuka a, "Physical metallurgy of Ti–Ni-based," *Progress in Materials Science,* p. 511–678, 2005.

[2] P. K. L. K. E. W. Kenneth E. Wilkes, "The fatigue behavior of shape-memory alloys," *JOM,* vol. 52, no. 10, pp. 45-51, 2000.

[3] T. Owen, "Shape Memory Alloys edited by Hiroyasu Funakubo, translated from the Japanese by J.B. Kennedy Gordon and Breach Science Publishers," *Robotica,* vol. 6, pp. 259-259, 1988.

[4] C. M. K. Otsuka, Shape Memory Materials, Cambridge university press, 1999.

[5] T. W. M. Wayman, "An introduction to martensite and shape," in *in Engineering Aspects of Shape Memory Alloys*, 1990, pp. 3-20.

[6] L. S. a. W. M. Huang, "Nature of the multistage transformation in shape," *Metal Science and Heat Treatment,* vol. 51, pp. 573-578, 2009.

[7] H. S. b. A. K. I. C. V. K. Ken Gall, "On the mechanical behavior of single crystal NiTi shape memory alloys and related polycrystalline phenomenon," *Materials Science and Engineering* , pp. 85-92, 2001.

[8] Y. Liu, "Detwinning process and its anisotropy in shape memory alloys," *Smart Materials, Proceedings of SPIE,* vol. 4234, pp. 82-93, 2001.

[9] C. M. W. K. Otsuka, "Shape Memory Materials," *Cambridge university press,* 1999.

[10] A. P. T. Duerig, "Ti-Ni shape memory alloys," *in Materials Properties Handbook: Titanium Alloys,* pp. 1035-1048, 1994.

[11] K. O. Y. S. S. Miyazaki, "Transformation pseudoelasticity and deformation behavior in a Ti-50.6at%Ni alloy," *Scripta Metallurgica,* vol. 15, pp. 287-292, 1981.

[12] K. S. K. Otsuka, "Pseudoelasticity and shape memory effects in alloys," *International Metals Reviews,* vol. 31, pp. 93-114, 1986.

[13] T. W. Duerig, "An engineer's perspective of pseudoelasticity," in *Engineering Aspects of Shape Memory Alloys*, 1990, pp. 369-393.

[14] N. Morgan, "Medical shape memory alloy applications—the market and its products," *Materials Science and Engineering,* pp. 17-23, 2003.

[15] K. O. a. K. Shimizu, "Pseudoelasticity and shape memory effects in alloys," *International Metals Reviews,* vol. 31, pp. 93-114, 1986.

[16] D. C. L. David A. Miller, "Influence of cold work and heat treatment on the shape memory effect and plastic strain development of NiTi," *Materials Science and Engineering,* pp. 161-175, 2001.

[17] K. N. M. D. S. T W Duerig, Engineering Aspects of Shape Memory Alloys, 1990.

[18] J. P. P. S. R. D. C. C. B. Malard, "In situ investigation of the fast microstructure evolution during electropulse treatment of cold drawn NiTi wires," *Acta Materialia,* vol. 54, p. 1542–1556, 2011.

[19] "R.S. Dennis, J.F. Tu," *Journal of materials processing technology,* vol. 199, p. 245–255, 2008.

[20] J. M. A. J. Birnbaum and Y. L. Yao, "The Effects of Laser Forming on NiTi Superelastic Shape Memory Alloys," *Journal of Manufacturing Science and Engineering,* vol. 132, no. 4, p. 041002, 2010.

[21] Y. B. J. V. X. Wang, "Laser annealing of amorphous NiTi shape memory alloy thin films to locally induce shape memory properties," *Acta Materialia,* vol. 53, no. 18, p. 4955–4961, 2005.

[22] Y. L. H. Y. B. S. S. T.-h. N. Q. Meng, "Functionally graded NiTi strips prepared by laser surface anneal," *Acta Materialia,* vol. 60, no. 4, p. 1658–1668, 2012.

[23] D. J. H. a. D. C. Lagoudas, "Aerospace applications of shape memory," *Journal of Aerospace Engineering,* vol. 221, pp. 535-552, 2007.

[24] S. A. Thompson, "An overview of nickel–titanium alloys used in dentistry," *international endodontic,* vol. 33, no. 4, p. 297–310, 2001.

[25] C. Song, "History and current situation of shape memory alloys devices for minimally invasive surgery," *Open Medical Devices Journal,* pp. 24-31, 2010.

[26] A. P. D. S. T. Duerig, "An overview of nitinol medical applications," *Materials Science and Engineering* , p. 149–160, 1999.

[27] M. A. S. L. G. Machado, "Medical applications of shape," *Brazilian Journal of Medical and Biological,* vol. 36, p. 683–691, 2003.

[28] F. M. Lorenza Petrini, "Biomedical Applications of ShapeMemory Alloys," *Journal of Metallurgy,* p. 15, 2011.

[29] T. Frank, "Medical Applications for Shape-Memory Alloys (SMA)," *Professional Engineering Publishing,* p. 31, 1999.

[30] T. Duerig, "Applications of shape memory," Vols. 56-58, pp. 679-692, 1990.

[31] D. H. T. D. K. M. D. S. a. C. W. J. Perkins, Engineering Aspects of Shape Memory Alloys, 1999.

[32] R. H. N. S. C. D. a. L. M. D. C. H. Beauchamps, European Conference on Smart Structures and Materials, Proceedings of the INT Conference Held in Glasgow, 1992.

[33] N. M. L. G. Song, "Applications of shape memory alloys in civil," *Eng.*

Struct, vol. 28, pp. 1266-1274, 2006.

[34] J. V. Humbeeck, "Non-medical applications of shape memory alloys," *Materials Science and Engineering,* p. 134–148, 1999.

[35] "Design optimization and uncertainty analysis of SMA morphing structures," *Smart Mater Struct,* 2012.

[36] M. N. T. S. M. Z. M. M. R. Sreekumar, "Critical review of current trends in shape memory alloy actuators for intelligent robots," *Industrial Robot,* vol. 34, no. 4, pp. 285-294, 34, Issue 4, 2007, Pages 285-294.

[37] S. R. M. E. E. Mohammad Mahdi Kheirikhah, "A Review of Shape Memory Alloy Actuators in Robotics," vol. 6556, pp. 206-217, 2011.

[38] Y.-C. L. M. T. Tao Tao, "Bio-inspired actuating system for swimming using shape memory alloy composites," vol. 3, no. 4, pp. 366-373, 2006.

[39] J. G. B. S. S. Stephen, "Design and fabrication of a bat-inspired flapping-flight platform using shape memory alloy muscles and joints," *Smart Mater Struct,* vol. 22, p. 014011, 2013.

[40] T. Yoneyama, H. Doi and E. K. a. H. Hamanaka, "effect of heat treatment with the mould on the superelastic property of NiTi alloy casting for dental application," *Frontiers of Medical and Biological Engineering,* vol. 10, no. 2, pp. 97-103, 2000.

[41] K. O. a. T. Kakeshita, "Science and technology of shape-memory alloys: new developements," pp. 99-100.